FINE MAPPING OF THE SPATIAL RELATIONSHIP BETWEEN ACUTE ISCHEMIA AND DENDRITIC STRUCTURE INDICATES A SELECTIVE VULNERABILITY OF LAYER V NEURONAL DENDRITIC TUFTS WITHIN SINGLE NEURONS *IN VIVO*

by

LAUREN ENRIGHT

B.Sc., McGill University, 2003

A THESIS SUBMITTED IN PARTIAL FULFILMENT OF
THE REQUIREMENTS FOR THE DEGREE OF

MASTER OF SCIENCE

in

The Faculty of Graduate Studies

(Neuroscience)

THE UNIVERSITY OF BRITISH COLUMBIA

August 2006

ABSTRACT

We have evaluated the spatial relationship between local blood flow and the structural integrity of layer 5 cortical neurons in YFP-H transgenic mice 2-10 h after stroke. Fortuitously, ischemic zones could be finely mapped with respect to dysmorphic YFP labelled axons and dendrites using histology since texas-red dextran used to measure blood flow *in vivo* was trapped within fixed ischemic vessels. Ischemic damage to layer 5 neurons located at the border of ischemia was contained within apical tuft dendrites and did not propagate to deeper dendrites despite the potential for diffusion of released cytotoxic factors. Dendritic damage decayed sharply with distance from the edge of ischemia (50% reduction in beaded dendrites within ~100 μm) and increased with time up to 6 h after stroke but not thereafter. Axonal damage also increased with time after the infarct but extended further laterally than dendritic damage, up to 600 μm from the stroke core. Apoptotic and necrotic cell death cascades were activated 6 h after stroke, however, only within 300 μm of the ischemic core. These data suggest that the axonal and dendritic circuitry of neurons located 300 μm outside of an ischemic zone can be relatively free of damage or commitment to cell death pathways suggesting that they may be in an ideal position to contribute to functional recovery. Given that ischemic damage may have a larger effect on circuitry involving superficial dendrites and projecting axons it is conceivable that surviving peri-infarct neurons may have unique structural and functional properties.

TABLE OF CONTENTS

LIST OF TABLES

LIST OF FIGURES

LIST OF ABBREVIATIONS

Ab = antibody
ADR = axonal damage rating scale
AMPA = α-amino-5-hydroxy-3-methyl-4-isoxazole propionic acid
ATP = adenosine triphosphate
Ca^{2+} = calcium
CCA = common carotid artery
Cl^- = chloride
d = day
DNA = deoxyribonucleic acid
ECA = external carotid artery
FITC = fluorescein iso-thiocyanate
g = gram
GAP-43 = growth associated protein 43
h = hour
ICA = internal carotid artery
i.p. = intraperitoneal
K^+ = potassium
MCA = middle cerebral artery
MCAO = middle cerebral artery occlusion
mg = milligram
min = minute
ml = milliliter
mM = millimolar
mm = millimeter
mW = milliwatt
Na^+ = sodium
NBM = nucleus basalis magnocellularis
nm = nanometer
NMDA = N-methyl D-aspartate
nNOS = neuronal nitric oxide synthase
PBS = phosphate buffered saline
PI = propidium iodide
PFA = paraformaldehyde
RB = rose bengal
TPA = tissue plasminogen activator
TR= texas red
TRP = transient receptor potential
μm = micrometer
v = volume
W = watt
w = weight
YFP = yellow fluorescent protein

AKNOWLEDGEMENTS

First and foremost, I would like to thank my supervisor, Dr. Timothy Murphy, for his expert technical advice, support and encouragement throughout the course of my Master's project. Tim's genuine devotion to science and ability to mutli-task is truly inspirational. He is a great mentor for any scientist.

I would like to thank Dr. A. El-Husseini for use of his Zeiss Meta confocal microscope on which the majority of my imaging was done, Dr. T.C. Saido for providing the 136kf α-spectrin antiserum, and Dr. T. Momoi for the m3D175 antiserum. I would also like to thank the members of my supervisory committee including Dr. Brian Macvicar, Dr. Jane Roskams, and Dr. Wolf Tetzlaff for their helpful suggestions on my project.

I would like to extend a big thank-you to all the members of the Murphy lab for providing unconditional help and advice with my experiments. Shengxiang Zhang was most helpful with tail vein injections and provided me with much of the brain tissue on which I performed my data analysis. Andy Shih and Ping Li were most influential in teaching me the technical ropes of animal research and Heidi Erb was always there to assist with experiments and answer my sometimes redundant questions. Finally, I could not have completed this project without the support and advice of Craig Brown, my fellow scientist and friend.

Last but certainly not least, I would like to thank my parents, Joanne Ferme and Michael Enright, for their encouragement and love throughout the course of my study, as well as my friends; Tara S., Nate B., Pam A., Kristy A., and Justin D and roommates Katie K., Carolyn D. and Belinda C. I couldn't have gotten through this degree without you guys. Merci à tous!

I. CHAPTER 1: INTRODUCTION

1.1. Clinical stroke and epidemiology

It is estimated that in the United States someone has a stroke every 45 seconds and one out of four of these people die. This translates into approximately 700,000 new stroke patients and 273,000 mortalities due to stroke per year (American Heart Association statistics, 2006). These numbers rank stroke as the third leading cause of death, behind diseases of the heart and cancer.

The risk of stroke in healthy adults over 55 is greater than one in six and women are even more prone to ischemic brain injury than men (Hurn et al., 2005). Factors which increase the risk of stroke include smoking and high blood pressure (Frizzell, 2005). The degree of remission after stroke depends on a variety of factors but behavioral outcome will ultimately depend on the severity of the neuronal damage (Mayo et al., 1999). Out of those individuals that survive their stroke, 50-70% regain functional independence, 15-30% remain permanently disabled and 20% require institutional care at three months after onset. The estimated cost of stroke in direct (hospital, nursing home, physicians, drugs) and indirect (loss of productivity and morbidity) finances amounts to 59 billion dollars per year (American Heart Association statistics, 2006).

1.2. An overview of the different types of stroke

Stroke results from the interruption of blood flow (ie. ischemia) to the brain (Gilroy, 2000). There are two main categories of stroke that are distinguished by the nature of the ischemia that is their cause: ischemic or hemorrhagic (Hossmann, 1998). Ischemic stroke, the most common type of stroke, occurs when a blood vessel becomes occluded and blow flow to the brain is partially or permanently interrupted. Focal stroke, global stroke and embolic stroke are the three main types of ischemic stroke. Permanent focal ischemia generally occurs when

there is a tear in an artery wall, causing platelets and clotting factors in the blood to aggregate within the artery thus impeding blood flow. This is also known as thrombotic stroke. Transient forms of focal ischemia also exist and result from severe vasospasms. The most common clinical cause of global ischemia is cardiac arrest where blood flow to the brain is completely interrupted. Embolic stroke differs from thrombotic stroke in that blood flow is obstructed by a traveling particle in a blood vessel, or embolus. Hemorrhagic stroke, also known as intracranial hemorrhage, occurs when a blood vessel in the brain ruptures, and blood escapes into the surrounding brain tissue. Although a more rare form of stroke, hemorrhagic stroke poses a greater risk for death and permanent disability than ischemic stroke (Rosamond et al., 1999).

1.3. The pathobiology of ischemic stroke

1.3.1. A cascade of cellular events

The brain is a highly metabolically active organ which consumes a large amount of oxygen and glucose. In stroke, cessation of blow flow and hence nutrients to the brain triggers an immediate cascade of cellular events that continue to evolve throughout time and space, leading to the demise of the brain tissue (Dirnagl et al., 1999). With energy depletion, first ion homeostasis and consequently membrane potential is lost, causing neurons to depolarize and excitatory amino acids to be released into the extracellular space (Katsura et al., 1994; Martin et al., 1994). Increased influx of Na^+ and Cl^- into the intracellular space also causes the passive influx of water into cells, leading to severe tissue edema (Heo et al., 2005). Increases in extracellular glutamate lead to the overactivation of NMDA receptors, resulting in increased intracellular Ca^{2+} levels (Park et al., 1989) and consequently activation of apoptotic and necrotic cell death cascades (Lipton, 1999). Calcium also triggers the activation of phospholipase A_2, cyclooxygenase and neuronal nitric oxide synthase (nNOS) which all contribute to the generation of free radicals, producing lipid peroxidation and membrane damage (Kristian and

Siesjo, 1998). Mitochondria are severely impaired by free radicals which cause disruption of the inner mitochondrial membrane. This results in the cessation of ATP production, the oxidation of proteins that mediate electron transport and the subsequent production oxygen free-radicals as well the release of cytochrome C which also contributes to the activation of apoptotic mechanisms (Fujimura et al., 1998). Oxidative stress and free radicals have also been shown to activate a number of receptors from the transient receptor potential (TRP) family of cation channels (Aarts and Tymianski, 2005), some of which are permeable to Ca^{2+} and contribute to increased intracellular Ca^{2+} and anoxic neuronal death (Aarts et al., 2003).

1.3.2. Tissue microenvironments after stroke

The cellular mechanisms triggered by ischemia are not necessarily uniform throughout the ischemic territory and whether a region of cortex will survive depends on a variety of factors such as the location and the duration of the ischemic insult. Typically, a stroke will result in an ischemic core of irreversibly damaged tissue, surrounded by a severely hypoperfused penumbra where cells are functionally impaired but still viable (Hossmann, 1994). In terms of perfusion parameters, the stroke core may be defined as the area in which blood flow is severely reduced to 20% of normal, or below 10mL/100g·min (Hossmann, 1994). If reperfusion does not occur naturally (through break-up of clots) or therapeutically (with a thrombolytic agent such as tissue plasminogen activator; TPA) within the critical time window of 3 -6 hours after the onset of stroke symptoms (Millan and Davalos, 2006), this severe reduction in blood flow will typically result in immediate cell death within the tissue that is supplied by the blocked artery. The nature of this cell death is usually considered to be necrotic and irreversible (Lipton, 1999). The ischemic penumbra is characeterized by a 60% decline in perfusion from control values, or to approximately 35mL/100g·min (Hossmann, 1994). Energy metabolism and ion homeostasis within this region is initially preserved; however, protein synthesis is surpressed (Hata et al.,

2000). Again, with reperfusion penumbral tissue may be rescued from infarction; however, if blood flow parameters do not return to near normal levels the cellular events triggered by the initial ischemic insult will result in the recruitement of penumbral tissue into the stroke core, an event which can continue up to days after the infarct (Ginsberg and Pulsinelli, 1994).

It has been shown that peri-infarct depolarizations are key mediators of the delayed neuronal death that occurs in penumbral tissue (Hossmann, 1996). These spreading depression-like depolarizations reflect large decreases in extracellular Na^+ and Ca^{2+}, and increases in extracellular K^+ and glutamate and they cause widespread damage by propagating throughout the entire cerebral hemisphere (Ashton et al., 1990). Na^+ channel blockers as well as NMDA and non-NMDA glutamate receptor antagonists have been shown to surpress perinfarct deplolarizations, thus reducing the final size of the infarct (Gill et al., 1992; Iijima et al., 1992). As survival of penumbral tissue is known to be positively correlated with the fuctional outcome of stroke patients (Furlan et al., 1996), it follows that the therapeutic suppression of peri-infarct depolarizations may lead to enhanced functional recovery after stroke.

1.3.3. Neuronal apoptosis

Apoptosis is a form of programmed cell death that is characterized by nuclear DNA condensation and fragmentation (Majno and Joris, 1995). Apoptotic cell death is also distinguished from necrotic cell death in that it is an energy dependant process that requires ATP and does not provoke inflammation of the surrounding tissue (Yamashima, 2004). Cytosolic cysteine proteases known as caspases are the key molecular players in the apoptotic cell death cascade and the activation of these caspases has been shown to be associated with apoptotic cell death after ischemic brain injury (Chen et al., 1998; Namura et al., 1998). Early activation of apoptotic cascades involve the pathways linked to caspase-8 and caspase-1; whereas, recruitment

of the penumbra into the stroke core primarily involves pathways linked to caspase-9 (Benchoua et al., 2001). Activated caspase-3 has been documented as early as 4 hours after reperfusion in a transient model of focal ischemia by MCAO (Ferrer et al., 2003) and this specific caspase isoform has also been shown to contribute to delayed apoptosis following the same model of transient focal ischemia (Chen et al., 1998). A further role for caspase-3 in ischemic cell death has been supported by evidence that inhibitors of caspase-3 activation reduce cell death up to 7 d after global ischemia (Chen et al., 1998).

1.3.4. Neuronal necrosis

Necrotic cell death generally occurs during neurodegeneration in response to distress from physical or chemical challenges. Necrosis may be differentiated from apoptosis on a variety of levels. The hallmark features of necrosis are mitochondrial and cell swelling, non-specific DNA fragmentation in the nucleus, and plasma membrane rupture (Majno and Joris, 1995). Further, necrosis is an ATP-independent process which incurs damage to the surrounding tissue as the intracellular contents of cells leak out into the extracellular space upon membrane rupture (Yamashima, 2004). Necrotic cell death is known to be mediated by calpain, a calcium-dependent neutral cysteine protease whose activation has been shown to be associated with brain ischemia (Yamashima et al., 2003). During ischemia, increases in intracellular Ca^{2+} lead to the activation of calpain which mediates cytoskeletal breakdown leading the loss of structural integrity resulting in cell death. It should be noted that calpain activation is not only specific to necrotic cell death as it also been shown to be associated with neuronal apoptosis (Nath et al., 1996; Wang, 2000).

1.3.5. Brain ischemia and neuronal cell death

Apoptosis and necrosis are two distinct forms of cell death that have both been implicated in ischemic brain injury (Majno and Joris, 1995; Lipton, 1999); however, a

controversy exists as to the relative contribution of these two cell death pathways following cerebral ischemia. It is generally accepted that following an ischemic event, apoptosis is the predominant form of cell death within the penumbra; whereas, neuronal necrosis is specifically localized to the infarct core (Aggoun-Zouaoui et al., 1998). Certain studies, however, have shown that supposed necrotic cells within the ischemic core show morphological, physiological and biochemical characteristics of apoptosis suggesting that apoptotic cell death is in fact the first cell death cascade to be activated within the infarct core after acute ischemia (Benchoua et al., 2001). In a photothrombotic ring model of stroke with spontaneous reperfusion both apoptotic and necrotic cell death cascades were shown to be activated within the well-defined region of severely reduced cerebral blood flow. Further, markers for apoptosis and necrosis have been shown to be expressed within the same set of ischemic neurons after transient and permanent MCAO (Unal-Cevik et al., 2004). Thus, it appears that postischemic neuronal death may involve a combination of apoptotic and necrotic processes even at the level of the individual neuron.

1.3.6. Structural changes to neurons

The ischemic cascade involves the activation of a number of proteolytic enzymes which ultimately lead to the breakdown of cytoskeletal and extracellular matrix proteins (Dirnagl et al., 1999). Thus it is understandable that as a result of ischemic damage, neurons will loose their structural integrity before progressing to a necrotic or apoptotic state of cell death. Focal, bead-like swelling of dendrites (also known as varicosity formation) consisting of collapsed cytoskeletal proteins and motor proteins has been shown to be a morphological response to ischemia (Hori and Carpenter, 1994) that precedes neuronal cell death (Takeuchi et al., 2005). Interestingly, this has been shown to be a reversible phenomenon after sublethal NMDA concentrations (Ikegaya et al., 2001), reperfusion (Zhang et al., 2005) or warming of previously

chilled brain tissue (Kirov et al., 2004). The induction of neuritic beading by activated microglia *in vitro* is thought to be mediated through NMDA receptor signaling as blockade of NMDA receptors abolishes the beading response (Takeuchi et al., 2005). As dendritic swelling has also been shown to be accompanied by AMPA receptor internalization (Ikegaya et al., 2001) it is thought that this pathological structural alteration to dendrites may be an early defensive response to excitoxicity.

Morphological changes to neurons following cortical damage have also been studied in depth at the level of individual synapses. In a comprehensive study (Gonzalez and Kolb, 2003), changes in the dendritic branching pattern and spine density of layer 5 pyramidal cells in the forelimb area were compared between 3 different models of stroke as well as between the affected and unaffected hemispheres. The resulting pattern of structural modifications to dendrites and spines of layer 5 neurons was found to be dependant on the site (affected vs. unaffected) as well as the type of stroke (aspiration lesion, devascularization, or MCAO) being investigated, illustrating that neuronal plasticity is highly sensitive to the nature of different brain lesions. Structural changes to spines following ischemia have also been studied *in vivo* where again, it would appear that different models of stroke produce different effects. In an endothelin-1 model of ischemia, a moderate reduction in blood flow (~50% supply) did not result in a significant disturbance of spines within 5 h; however, in the cortical photothrombosis model, there was a rapid deterioration of spine and dendrite structure within 10 minutes of the ischemic insult (Zhang et al., 2005). Interestingly, reperfusion was associated with the recovery of dendrite and spine structure and not further damage.

It is known that neurons display plastic properties after stroke; however, it would appear that not all subsets of neurons are equally plastic after brain injury. Following unilateral lesions

in the forelimb region of the rat sensorimotor cortex, the dendritic arborization of layer 5 pyramidal neurons was found to increase in a time-dependant manner in the contralateral homotopic cortex until 2-3 weeks after the lesion (Jones and Schallert, 1992). In agreement with this, morphological assessment of dendrites in layer 2/3 and layer 4 spiny stellate cells in the contralateral hand region of adult primates indicated expansion of the distal regions of the dendritic arbor with few changes proximally after denervation (Churchill et al., 2004). In contrast, lesions of the nucleus basalis magnocellularis (NBM) in aged rats indicated a decrease in the dendritic branching pattern of layer 2/3 frontal cortical neurons; however, this affect was also found to be most pronounced in dendritic material distal to the soma (Wellman and Sengelaub, 1995).

These studies are consistent with the idea that cortical damage evokes changes in the morphology of neurons and that these changes differ between populations of neurons. It would appear that neurons located within the damaged hemisphere retract their dendritic processes whereas those located on the contralateral hemisphere expand. Further, it seems that in both cases, changes in dendritic arborization are most prominent within the distal regions of the dendrite whereas the more proximal regions of the dendrite appear to be minimally affected.

1.4. Neural correlates of recovery of function after stroke

Acutely, ischemia induces a cascade of cellular events leading to immediate neuronal damage within the stroke core. The effects of stroke; however, continue to evolve beyond the initial ischemic insult in both time and space. Molecular changes as well as changes in the structure and physiology of cortical circuits surrounding the lesioned tissue have been documented in the months following stroke (Sharp et al., 2000; Weinstein et al., 2004) and these have been suggested to be a neural substrate for stroke recovery (Ward, 2005).

The ability of the adult brain to reconnect with partially damaged brain areas after stroke is thought to be associated with axonal sprouting. Evidence for axonal sprouting after stroke has come from studies of growth associated protein 43 (GAP-43), a membrane phosphoprotein important in linking membrane signaling to actin cytoskeleton modification (Benowitz and Routtenberg, 1997). GAP-43 has been shown to be directly related to axonal sprouting as overexpression of this protein induces enhanced sprouting after lesions and knockdown of GAP-43 reduces axonal sprouting (Benowitz and Routtenberg, 1997). Interestingly, GAP-43 has been shown to be highly elevated in human brain tissue following stroke (Ng et al., 1988) as well as in the tissue bordering the infarct in rats after MCAO (Stroemer et al., 1993) and photothrombotic ischemia (Wu et al., 2002). Thus it appears that GAP-43 plays an essential role in the remodeling and repair of neurons after brain ischemia.

Further evidence for neuroplasticity in peri-infarct regions of partially damaged synaptic structures comes from studies looking at synaptophysin immunoreactivity as a measure of changes in the number of synapses. Two months after recovery from MCAO, rats were found to have increased levels of synaptophysin in regions of cortex surrounding the infarcted area (Stroemer et al., 1992) suggesting that synaptogenesis is occurring in the perilesion cortex. In another study by the same group, the maximal increase in synaptophysin was found to occur after increases in GAP-43 following ischemia, and the temporal pattern of both of these processes was found to correlate with behavioral recovery of rats (Stroemer et al., 1995). Hence neurite growth followed by synaptogenesis may contribute to recovery of function after stroke.

Axonal sprouting following stroke has also been shown to be associated with remodeling of cortical sensory maps, again, a potential substrate for stroke recovery (Carmichael et al., 2001). Following an ischemic event, neurons in areas distant from the lesion site as well as those

near the infarct core have been shown to have the ability to form new synaptic connections (Dancause et al., 2005). As a consequence, the brain can recruit adjacent areas of the somatotopic map such that a cortical region devoted to one specific function may grow in size. As an example of this, it has been shown that the recovery of hand use after human stroke correlates with an increase in the hand region of the motor cortex and that the degree of plasticity of this motor map, in turn, correlates with the level of functional recovery (Traversa et al., 1998). This has also been shown in a study with primates where microlesions abolished the cortical region specifically involved in a small-object retrieval task but recovery of function was associated with a reemergence of an even larger region of motor cortex devoted to this skill (Xerri et al., 1998). Other studies have also linked changes in brain morphology after stroke to functional outcome. In one study, damage to the sensorimotor cortex resulted in an increase in dendritic arborization of layer V pyramidal neurons in the contralateral homotopic cortex and this change was shown to correlate closely with behavioral events (Jones and Schallert, 1994). Specifically, expansion of the dendritic arbor in the hemisphere contralateral to the lesion was associated temporally with increased use of the unaffected forelimb for postural and exploratory movements, and pruning of the dendrites at a later time point occurred at the same time as the animals returned to a more symmetrical use of the forelimbs.

In line with the apparent plasticity of the brain following stroke contributing to recovery of function is the ability of the brain to respond to behavioral therapies and environmental enrichment. It is well known that the even the adult brain is particularly sensitive to its environment and that this may have profound effects on neurogenesis, synaptogenesis, and hence the strength of connections between neurons (Lledo et al., 2006). Behavioral therapy following stroke is known to improve functional outcome and this has been shown to be related to functional reorganization of the motor cortex following injury and recruitment of adjacent

regions of the motor map (Nudo et al., 1996). Similarly, exposure to an enriched environment before or after focal ischemic injury has also been shown to result in improvement on sensorimotor tasks (Ohlsson and Johansson, 1995; Johansson and Ohlsson, 1996). Environmental enrichment and task-specific rehabilitive therapy after focal stroke have both been shown to be associated with enhanced dendritic complexity and length, and thus improved functional outcome in these cases is thought to be mediated by the augmentation of neuronal plasticity after stroke (Biernaskie and Corbett, 2001). Taken together, these studies indicate that rehabilitive therapies have the ability to remodel the neuronal circuitry surrounding injured tissue and this neuroanatomical reorganization may contribute to the recovery of motor deficits following stroke.

1.5. Animal models of stroke

The development of reliable and reproducible animal models of cerebral ischemia which mimic most features of human clinical stroke as best as possible is of key importance for the systematic study of the pathophysiology of stroke. As outlined above, there are many different types of stroke thus it follows that there have been many different stroke models that have been devised (Table 1-1). Each model of stroke produces a lesion of different size and affects different cortical areas. Further, the choice of model also has an impact on the nature of the post-injury pathology as well as on functional recovery or compensation mechanisms. Thus it is evident that it is important to be aware of the pathophysiological differences between animal models in order to choose a model that is best suited to answer the hypothesis being tested. In this study, we have chosen to use two different animal models of stroke, namely the rose bengal (RB) cortical photothrombosis model and the middle cerebral artery occlusion model (MCAO).

Model	Type of stroke	Strengths	Weaknesses	Reference
bilateral common carotid artery occlusion	global stroke	- simplicity of surgical manipulation	- high level of mortality in animals and seizures	Traystman, 2003
MCAO	permanent or transient focal ischemia	-models the ischemic penumbra -good for studies of neuroprotective therapies	-subarachnoid hemorrhage -hypothalamic damage -damage to functionally diverse brain regions	Bederson et al., 1986; Kuge et al., 1995; Schmid-Elsaesser et al., 1998
embolic MCAO	embolic ischemia	-immediate perfusion deficits -no hypothalamic damage -lesion size easily manipulated	-time course of lesion expansion is slower - lesions are more variable in size and location	Miyake et al., 1993; Mayzel-Oreg et al., 2004
endothelin-1	focal ischemia	-dose dependent blood flow reduction -highly localized lesions -white matter ischemia -no BBB breakdown -little tissue edema	-large penumbra	Masaki and Yanagisawa, 1992; Fuxe, 1997; Hughes, 2003
photo-thrombosis	focal ischemia	-size of infarct can closely resemble human condition -highly localized lesions -minimally invasive	- minimal penumbra region	Watson et al., 1985; Lee et al., 1996; Van Hoecke et al., 2005

Table 1-1. Summary of the most widely used animal models of stroke.

1.5.1. Cortical photothrombosis

The photothrombotic stroke model is a unique model of focal ischemia in that it utilizes a photosensitize dye such as rose bengal to induce a highly localized lesion within the cortex (Watson et al., 1985). When irradiated by light through the intact skull, the dye injected either through the tail vein or abdomen (Kim et al., 2000) of the animal undergoes a photochemical reaction leading to the release of singlet oxygen, causing damage to the vascular endothelium and ultimately leading to the formation of a thrombus thus impeding blood flow (Dietrich et al., 1987). The extent of damage to the targeted cortical areas can be precisely manipulated in this

model by controlling the intensity, duration, shape and position of the irradiating beam as well as the dose of photosensitive dye (Lee et al., 1996).

Cortical photothrombosis is a great tool for studies of stroke because, technically, it offers many advantages that other stroke models don't. First and foremost, the potentially small size of the infarct produced by this model makes it closely resemble the human condition, a characteristic that many of the other models lack. Human strokes are generally small in size, ranging from 28-80mm^3 which translates into 4.5-14% of the ipsilateral hemisphere (Carmichael, 2005). The size of photothrombotic lesions will vary depending on experimental factors, however in previous studies this has ranged from 14-69mm^3 corresponding to 9.9- 29.8% of the ipsilateral hemisphere (Shanina et al., 2005; Van Hoecke et al., 2005). Another advantage of the cortical photothrombosis model is that there is little inter-animal variation in the size of the cortical infarct, making the model well suited for replicate studies of pharmacotherapy (Markgraf et al., 1993). Further, the simplicity and minimal invasiveness of the surgical manipulations involved in this technique make for excellent survival of the animals (Van Hoecke et al., 2005). This is also ideal for *in vivo* imaging studies where it is possible to induce stroke while imaging the animal simultaneously. Probably the best advantage this model has to offer is its adaptability in terms of the region of infarct. As previously mentioned, photothrombosis allows for the localization of a stroke within distinct subdivisions of the cortex by manipulating the region of the skull being illuminated. This makes it possible to study the recovery of function after insults to a particular sensory modality. For example, by localizing a stroke within the forelimb area of the motor cortex, animals may then be tested on a forelimb motor reaching task to assess recovery and compensatory mechanisms (Metz et al., 2005). In human stroke, behavioral impairments are the result of damage to a particular neuronal circuit responsible for a

given brain function. Thus this model is relevant to clinical studies assessing ischemic deficits and rates of behavioral recovery.

One of the criticisms of this model is that the lesions are induced with such a sharp border that there is generally little local collateral blood flow and thus a minimal penumbra region, one of the defining characteristics of human stroke. One way to overcome this issue is to use a ring filter placed over the laser during photoactivation to create a central area within the lesioned cortex thus modeling a region of peri-infarct cortex (Hu et al., 2001). In the photothrombotic ring stroke model the ring lesion region is the central area at risk and the severity of the injury can be modulated by changing the intensity of the irradiation (Wester et al., 1995). By using low-intensity irradiation with a thin laser beam spontaneous reperfusion may occur between 48 h and 72 h after stroke onset (Gu et al., 1999). In contrast, high ring beam intensity produces consistent lack of reperfusion (Hu et al., 1999).

Another concern with the photothrombotic stroke model arises from the physiology of the photochemical insult. Activation of the rose bengal dye produces free radicals (singlet oxygen) which initiates disruption of the endothelial walls leading to substantial local vasogenic and cytotoxic edema (Watson et al., 1985; Gajkowska et al., 1997). Free radical induced neuronal damage, swollen cells, and leaky vessels more closely resemble traumatic brain injury models than human focal stroke (Albensi et al., 2000; Schneider et al., 2002). Despite this, studies have shown that the cellular cascades initiated by photothrombotic ischemia resemble those in other more classical models of stroke. Photothrombotic infarction has been shown to trigger spreading depression in distant brain regions (Dietrich et al., 1994), and NMDA and AMPA receptors have also been shown to be involved in the photothrombotically induced ischemic cascade (Yao et al., 1994; Umemura et al., 1997).

1.5.2. Middle cerebral artery occlusion (MCAO)

The MCAO model of focal ischemia has been in use since 1975 (Robinson et al., 1975). Many different techniques of occluding the MCA exist such as cauterization via a craniotomy (Tamura et al., 1981) and photothrombosis (Markgraf et al., 1994); however, the most widely used model of MCAO is the intraluminal thread model (Longa et al., 1989). In this technique, occlusion of the MCA is achieved by first transecting the external carotid artery (ECA) so that a suture may be passed through the internal carotid artery (ICA) to lodge in the junction of the anterior and middle cerebral arteries (Fig. 1-1). The suture can be left in place for variable durations and then removed to produce reperfusion. The most common durations of suture occlusion of the MCA in the rat are 60, 90, and 120 minutes and permanent occlusion (Carmichael, 2005). More recently, a new adaptation to the technique has been devised where the intraluminal sutures are coated with poly-L-lysine, a polycationic polymerized amino acid (Belayev et al., 1996). This modification was found to reduce subarachnoid hemorrhage and premature reperfusion, leading to more consistent infarct volumes.

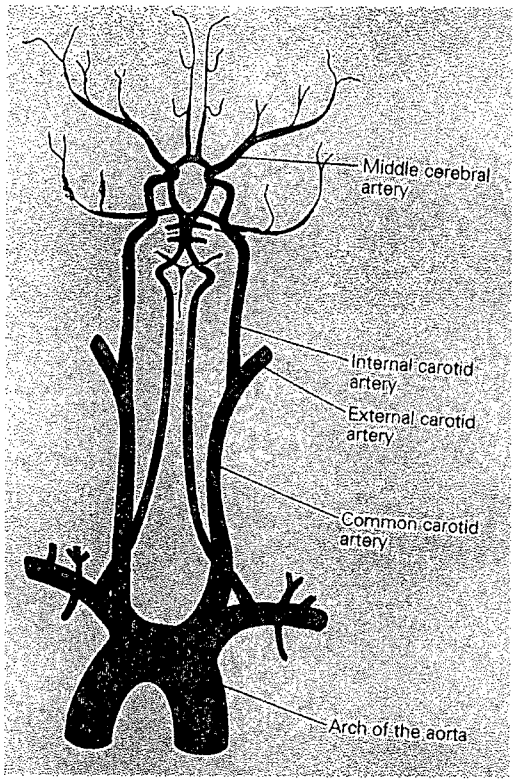

Figure 1-1. Schematic diagram illustrating the arteries involved in the MCAO procedure.

In the MCAO model of focal ischemia, occlusion of the middle cerebral artery (MCA) is achieved by first transecting the external carotid artery (ECA) so that a suture may be passed into the internal carotid artery (ICA) to lodge in the junction between the ICA and the MCA. (figure adapted from Kandel et al., 2000)

The main advantage of the MCAO stroke model lies in its resulting pattern of cell death which is consistent with the concept of an ischemic penumbra, a hallmark feature of human stroke. In MCAO with reperfusion, the striatum remains densely ischemic as thus serves as an ischemic core whereas the overlying cortex returns to control blood flow values, creating a region of delayed, progressive neuronal death or an ischemic penumbra (Takagi et al., 1995). The ischemic penumbra is a salvageable region of cell death which has serious implications for the study of neuroprotective therapies (Cheng et al., 2004).

As with the photothrombosis model, there are several concerns with the MCAO model of stroke. Firstly, the model has been consistently shown to produce subarachnoid hemorrhage, leading to a bilateral reduction in cerebral blood flow (Bederson et al., 1995; Kuge et al., 1995; Schmid-Elsaesser et al., 1998). This may decrease the pathophysiological relevance of the model. Second, hypothalamic damage is evident in models where suture occlusion lasts 60 minutes or longer (Li et al., 1999). Hypothalamic ischemia is of concern because it leads to a hyperthermic response for a minimum of a day during the recovery period of the animal which may exacerbate cell death (Li et al., 1999). Further, hypothalamic ischemia is rarely seen in human stroke. Thirdly, the intraluminal thread model of MCAO requires the ECA to be cut before thread insertion, a procedure which interrupts blood flow to the muscles of mastication and swallow, producing difficulty in eating in animals and weight loss. Although this practice has no repercussions on the size of the infarct, it was associated with poorer performance on post-stroke behavioral measures (Dittmar et al., 2003). Finally, because the MCAO stroke model creates damage in many functionally diverse brains regions it is likely to produce complex deficits in a wide range of sensory modalities. Thus the MCAO model of focal ischemia may be a more difficult model to study the contribution of specific neuronal circuits to the recovery of function after stroke.

1.6. Research hypothesis and rationale

Focal stroke is characterized by an ischemic core surrounded by a severely hypoperfused penumbra (Hossmann, 1994). Tissue at the core of a stroke is generally considered to be irreversibly damaged; however, penumbral tissue may still be viable as here, only a fraction of cells are lost (Kato and Kogure, 1999; Sharp et al., 2000). The evolution of cell death in the ischemic penumbra is a highly dynamic process, with the incidence of dying cells increasing with time after infarction (Jones et al., 1981). Ultimately, whether or not a penumbral cell will survive depends on its proximity to the ischemic vasculature and the degree/duration of ischemia. **Although survival of penumbral tissue has been previously evaluated, it is not known whether there is acute damage to the fine axonal and dendritic circuitry within this region *in vivo* and how this relates to ongoing apoptotic and necrotic cell death.**

Previously using 2 photon-*in vivo* imaging of layer 5 neurons in YFP expressing transgenic mice in our lab, we have shown that severe cortical ischemia produced by local photothrombosis leads to a widespread loss of cortical tuft dendritic structure within minutes (Zhang et al., 2005). **Here, we wish to uncover whether this *in vivo* damage will propagate into the deeper dendritic and axonal compartments of these same neurons as well as what the spatial and temporal pattern of this ischemic damage will be.** Examination of the integrity of tissue immediately adjacent to the infarct is important as this is where changes such as adaptive neuronal plasticity (Xerri et al., 1998; Dancause et al., 2005) and circuit reorganization (Carmichael et al., 2001) that underlie functional recovery have been shown to occur. **By defining the extent as well as the time course of axonal and dendritic ischemic damage within the penumbra we wish to establish how much of the peri-infarct circuitry is salvageable and thus may contribute to recovery acutely after stroke.**

II. CHAPTER 2: MATERIALS AND METHODS

2.1. Animals

Adult, C57BL/6 YFP expressing transgenic mice (H-line; (Feng et al., 2000) aged 3-5 months and between 25-32 g were used for all experiments. These animals were purchased from The Jackson Laboratory (Bar Harbor, ME) and bred at the University of British Columbia animal facilities. Protocols were approved by the Canadian Council for Animal Care and the University of British Columbia Animal Care Committee. All experiments were conducted in strict accordance with the National Institutes of Health *Guide for the Care and Use of Laboratory Animals*.

2.2. Stroke models

2.2.1. Rose bengal photothrombosis

For the majority of experiments we used the rose bengal (RB) cortical photothrombosis model of stroke. This model is minimally invasive and allows for very reproducible lesions (Watson et al., 1985). Before induction of stroke, animals were first prepared for *in vivo* 2-photon imaging as in Zhang et al., 2005. Animals were anesthetized with an intraperitoneal (i.p.) injection of urethane (0.12% w/w, supplemented at 0.02% w/w as needed) and supplemented with 2 mM glucose in PBS (0.2-0.3 ml, i.p., every 1 h). Body temperature was monitored with a rectal temperature probe and maintained at 37°C using a heating pad and feeback regulation from the probe. A 2 x 2 mm^2 cranial window was made over the somatosensory cortex at coordinates of -0.8 mm dorsal and 2.0 mm lateral from bregma, leaving the dura intact. A stainless-steel chamber that surrounded the craniotomy was glued to the skull with Krazy Glue (Elmer's Products, Columbus, OH). To reduce movement artifacts, the area between the chamber and the skull was filled with dental acrylic (Kleinfeld and Denk, 2000). The exposed cortical surface and chamber were filled with 2% (w/v) agarose (diluted in PBS or a HEPES-buffered

artificial CSF) and sealed by a cover glass (#1). To induce stroke, RB (0.03 mg/g mouse, diluted to 10 mg/ml in PBS) was injected into the mouse via the tail vein using a 28 ½ gauge needle after warming the tail with a lamp. Photoactivation of the dye was then achieved by focusing green light (535 ± 25 nm; ~3 mW) from a HBO 100 W arc lamp on the brain surface for 1-2 minutes through a 10x, 0.3 numerical aperture objective. The area of light reaching the exposed cortex was limited by the field aperture to ~0.5 mm^2. In all experiments, the area and depth of ischemic vessels was greater than the expected area (~0.5 mm^2) and depth of photoactivation (~12 μm full width at half maximal, given a 0.3 numerical aperture air lens) due to diffusion of clots or clot-inducing factors. In some cases, a craniotomy was not used and animals were also not imaged using the 2-photon microscope. In these animals the skull overlying the RB photoactivation area was thinned using a dental drill and photoactivation was performed through the thinned bone. Both the thin skull and craniotomy preparations produced lesions of similar size. Sham stroke operated animals that underwent the same craniotomy procedure (in the same location as stroke animals) and laser exposure (1-2 minutes) without injection of RB dye were used as controls.

2.2.2. Middle cerebral artery occlusion (MCAO)

For the middle cerebral artery occlusion (MCAO) model of stroke ischemia-reperfusion was induced using a modified version of the intraluminal suture method as described previously in rats (Longa et al., 1989). Briefly, anesthesia was induced with urethane (0.12% w/w) and body temperature was maintained at 37 ± 0.5°C using a heating pad and feedback regulation from a rectal temperature probe. Animals were place in a supine position and an incision was made along the midline of the ventral side of the neck. First, a 5-0 silk suture (Ethicon, Markham, ON, Canada) was used to block the common carotid artery (CCA) on the side of the MCA to be occluded. Then, two sutures were placed around the external carotid artery (ECA) and a heat coagulator was used to cauterize the ECA between them. This allowed for the ECA to be more

accessible during insertion of the suture. After blocking the internal carotid artery (ICA) with a micro-aneurysm clip (Harvard Apparatus, Holliston, MA), a small hole was cut in the ECA in which a 5-0 poly-L-lysine coated Dermalon monofilament nylon suture (Sigma, St. Louis, MO) was inserted. After removing the micro-aneurysm clip, the suture was pushed into the ICA until a mild resistance was felt, approximately 10 mm from the ICA/ ECA bifurcation and at a position past the junction of the MCA. At this point the suture around the CCA was loosened and the ventral neck skin was sutured. After 30-60 minutes of ischemia the skin was reopened and the suture retracted. Animals were sacrificed and perfused 90-300 minutes later. Although ischemia was reliably induced in 3 animals and confirmed by 2-photon imaging of blood flow, we only observed partial reperfusion in all cases.

2.3. *In vivo* 2-photon imaging

Mice were maintained under urethane anesthesia for the entire imaging session. Animals were fitted into a custom-made two-photon microscope. 2-photon excitation was performed with a Coherent Mira 900 Ti-sapphire laser pumped by a 5 W Verdi laser and was tuned to 920 nm to excite YFP as previously described (Zhang et al. 2005). Images were acquired by custom software (Igor) and by using an Olympus IR-LUMPlanFl water-immersion objective (60x, 0.9 numerical aperture). Using 0.2 μm fluorescent beads we estimated the lateral resolution to be 0.5 μm (measured as the width of the point spread function at ½ maximal fluorescence intensity). For *in vivo* time-lapse imaging of dendritic structure, multiple Z-series were taken at the indicated time intervals over 5 h. The spacing of successive Z-images was 1.0 μm and provided sufficient overlap between sections as the axial resolution of the imaging system at the settings used was ~2.0 μm. The imaged dendrites were typically within 100 μm of the pial surface and therefore in layer 1. The images were taken with a pixel size of 0.13 μm, typically spanning a 140 x 140 μm area, and were the average of 3 frames. Stroke was confirmed by *in vivo* 2-photon

imaging of blood flow as previously described (Zhang et al. 2005). Blood plasma was labeled through a tail-vein injection of a 0.1 ml bolus of 5% (w/v) fluorescein iso-thiocyanate (FITC)-labeled dextran (500 kDa) or texas-red (TR) dextran (70 kDa) in PBS. The velocity of red blood cells was then measured from repetitive line scanning along the central axis of a capillary (Kleinfeld et al., 1998) before and after activation of RB to confirm that blood flow was completely blocked.

2.4. Staining and immunohistochemistry

All staining and immunohistochemistry was performed on floating, 100 μm thick coronal sections of YFP expressing transgenic mice. Propidium iodide (PI; 10μM; Sigma, St. Louis, MO) was diluted in 0.3% Triton X-100 in PBS and incubated at room temperature for 1 hour. Sections were rinsed three times for 10 min in PBS prior to mounting with Fluoromount-G and No. 1 glass coverslips (Fisher Scientific, Edmonton, AB, Canada). Anti-m3D175 antiserum against the cleavage site of caspase-3 (a generous gift of Dr. T. Momoi) was diluted in 1:1000 in Ab buffer (3% bovine serum albumin and 0.3% Triton X-100 in PBS) and incubated overnight at 4 °C. For detection of calpain activation we used antiserum against the 136kf N-terminal fragment of α-spectrin (a generous gift of Dr. T. Saido), diluted to 1:500 in Ab buffer. Sections were first incubated at 80 °C for 30 min in 10 mM sodium citrate (pH 8.5) and then rinsed for 5 min in PBS prior to anti-136kf antibody incubation, also overnight at 4 °C. All sections were rinsed three times for 5 min in PBS after primary Ab incubation and then incubated with a goat anti-rabbit IgM Alexa 546-conjugated secondary antibody (Molecular Probes, Eugene, OR; 1:1000) for 1 h at room temperature. Sections were rinsed three times for 10 min in PBS prior to mounting. Fluorescent images were captured using a Zeiss LSM Meta 510 confocal microscope and analyzed using NIH ImageJ software.

2.5. Confocal microscopy on fixed coronal sections

2 h, 6 h, or 10 h after induction of stroke and (in most cases) *in vivo* 2-photon imaging animals were overdosed with sodium pentobarbital and then transcardially perfused with PBS followed by 4% paraformaldehyde (PFA) in PBS. After brains were post-fixed in 4 % PFA for 2 days, 100 μm sections were cut coronally on a vibratome and every fourth section was mounted on a glass slide and coverslipped with Fluoromount-G (Southern Biotechnology Associates Inc.) mounting solution. Those sections that contained the sham or photoactivated area were then used for imaging on a Zeiss LSM Meta 510 confocal microscope. For the analysis of the spatial spread of ischemic damage medium resolution (512 x 512) tiled images (5 X; 5 Y) of the ischemic and non-ischemic hemisphere were taken with a 20x, 0.5 numerical aperture objective. An Argon 1 laser was used at 514nm to excite the YFP signal and a He/Ne1 laser was used at 543 nm to excite the TR-dextran. Emission filters were set to 530-560nm for the YFP signal and 595-650 nm for TR-dextran. The same excitation and emission imaging parameters used for collection of the TR-dextran signal were also used for imaging of propidium iodide (PI) staining and immunohistochemical markers, where the secondary antibody was alexa 546. To examine fine dendritic structure, 2 channel, high resolution (1024 x 1024, 0.143 μm pixels) z-stacks (with 1 μm spacing between sections) were taken with a 63x, 1.2 numerical aperture water immersion lens throughout the length of the dendrite, starting at the level of the cell soma and extending to the cortical tuft dendrites at the surface of the cortex. These same image collection parameters were also used for imaging of PI, anti-m3D175, and anti -136kf α spectrin staining. Here, images were taken only at the level of the layer 5 neuron cell soma, and images were collected in adjacent 150 μm bins, starting 150 μm within the stroke core and extending 450 μm laterally throughout the adjacent peri-infarct cortex (4, 150 μm bins in total).

2.6. Image analysis

Image analysis was performed using NIH ImageJ software (http://rsb.info.nih.gov/ij/). To reduce photon and photomultiplier tube noise, a median filter (radius, 1) was applied to all images. For the analysis of the laminar distribution of ischemic damage throughout individual dendrites maximum intensity projections of filtered z-stacks were tiled together using Adobe Photoshop 7.0 software. Maximum intensity filtered z-stacks were also used for the analysis of cell viability with PI, anti-m3D175, and anti -136kf α spectrin immunohistochemical markers,

2.6.1. Spatial spread of ischemic damage to dendrites

For the analysis of the spatial spread of ischemic damage to dendrites a grid with tiles measuring 100 μm x 100 μm was placed over 20x tiled images of the ischemic hemisphere. The ischemic interface (border between ischemic and non-ischemic tissue) was defined as the vertical interface where 10% or less of total vessels spanning cortical layers 1-5 were ischemic (those vessels with TR-dextran caught within them) and was demarked with a line. Each dendrite was then scored as being beaded or normal. A beaded dendrite was defined as an apical dendritic shaft with 2 or more periodic dendritic constrictions resembling beads on a string. Dendritic beading was counted laterally across the cortex in 100 μm bins, beginning at the ischemic interface and ending 500 μm away and this analysis was performed between 50-100 μm below the surface of the cortex. The % of beaded dendrites of all dendrites counted (in each 100 μm bin) was calculated for each of 3 coronal sections per animal at three different time points: 2 h, 6 h, and 10 h after stroke. Dendrites were also counted in five, 100 μm bins on the non-ischemic hemisphere of stroke animals (in the contralateral homotypic cortex) as well as in sham stroke animals (in the somatosensory cortex). The total number of dendrites (per 100 μm bin) in the non-ischemic hemisphere and in sham stroke animals did not differ from the total number of

dendrites counted in the ischemic hemisphere. Also, no beaded dendrites were found in the non-ischemic hemisphere or in sham stroke cortex.

2.6.2. Spatial spread of ischemic damage to axons

For analysis of the spatial spread of axonal damage of layer 5 neurons, an axonal damage rating (ADR) scale was for devised as follows: 0= no axon damage (all axons are intact), 1= minor damage (~25% of axons beaded), 2= moderate damage (~50% of axons beaded), and 3= severe damage (~75% of axons beaded or complete loss of axonal integrity) (Fig. 2-1). A grid with tiles measuring 100 μm x 100 μm was placed over 20x tiled images of the ischemic hemisphere and the edge of the stroke core (where TR clotted vessels ended) was demarked with a line. A number (0-3) was then assigned to each tile of axons (immediately below the cell bodies) starting at the ischemic interface and extending 800 μm laterally throughout the axons of layer 5 neurons. 3 coronal sections per animal were analyzed at three different time points: 2 h, 6 h, and 10 h after stroke, and an average ADR was calculated for each animal at every time point.

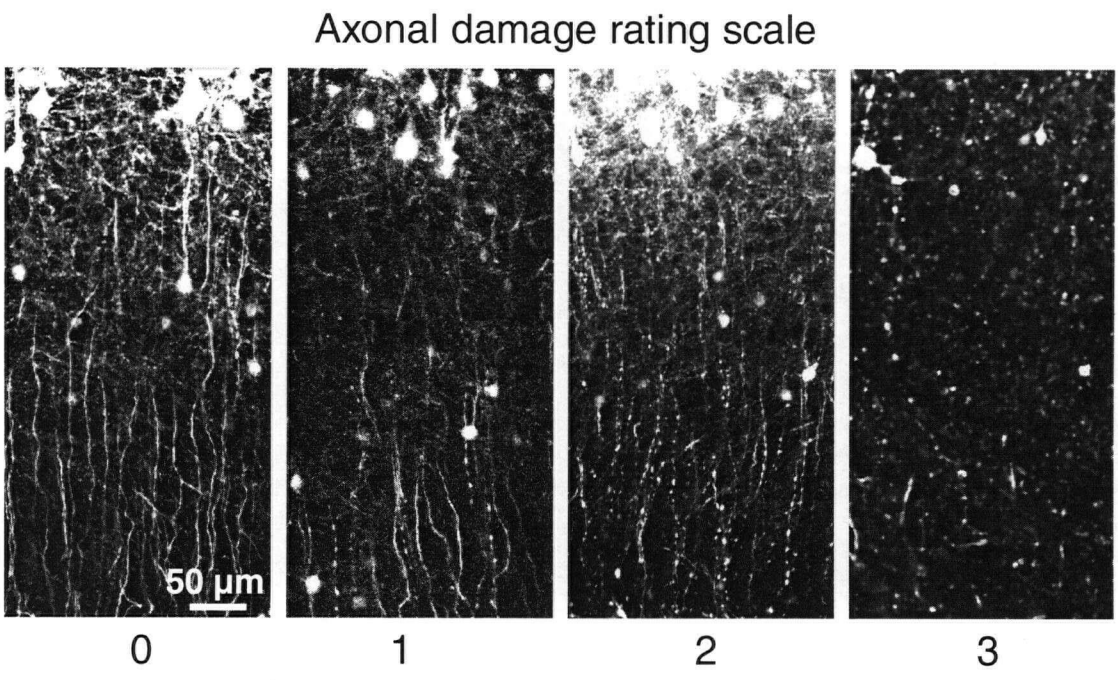

Figure 2-1. Examples of the axonal damage rating scale.

For the analysis of the spatial spread of ischemic damage to axons of layer 5 neurons a scale was for devised as follows: 0= no axonal damage (all axons are intact), 1= minor damage (~25% of axons beaded), 2= moderate damage (~50% of axons beaded), and 3= severe damage (~75% of axons beaded or complete loss of axonal integrity).

2.6.3. Analysis of YFP nuclear size

Propidium iodide (PI) is a fluorescent dye that binds specifically to DNA. As the dye is not permeant to live cells it will only stain cells with a compromised plasma membrane and thus it is generally used to detect dead cells within a population. In this study because we used PI on fixed and permeabilized brain tissue, all cells were labeled with PI so we chose to measure the size of a cell's nucleus as a measure of its integrity. First, we used 2 channel (red and green) merged images to determine which cells were labeled with YFP. These images were then split

into their respective red and green channels and the red channel was used for the measurement of nucleus size. The height and width of YFP cell nuclei were measured using Image J software and the formula (height/2 * width/2)* 3.14 was used to calculate the nucleus area. The average nucleus size of all YFP cells located within each 150 μm bin was calculated for each of 3 slices from 3 different animals that had been sacrificed 6 h after stroke induction. YFP cells located on the non-ischemic hemisphere of each animal were used as a control.

2.6.4. Analysis of markers of apoptotic and necrotic cell death

We used anti-m3D175 antiserum against the caspase-3 cleavage site (Urase et al., 2003) to detect activation of caspase-3, a cytosolic cysteine protease whose activation has been shown to be associated with apoptotic cell death after ischemic brain injury (Chen et al., 1998; Namura et al., 1998). To investigate the activation of necrotic cell death mechanisms 6 h after ischemia, an antibody against the 136-kDa fragment of calpain-mediated α-spectrin breakdown was used, as this specicifc α-spectrin breakdown product is only generated during neuronal necrosis making it a specific marker for this form of cell death (Takano et al., 2005). 2 channel (red and green) merged images were used to count the number of YFP cells that were labeled with either the apoptotic or necrotic marker. Additionally, the total number of YFP cells within each 150 μm bin was counted and the expression of anti-m3D175 and 136kf α-spectrin positive cells was represented as a percentage of total YFP cells. Again, a total of 3 slices from each animal were used for the analysis. Images of the cell somas of YFP neurons on the non-ischemic hemisphere of each animal as well as in sham control animals did not reveal any anti-m3D175 or 136kf α-spectrin positive cells. We also performed an investigation of anti-m3D175 and 136kf α-spectrin staining in animals at 2 h and 10 h after stroke; however, there were some technical issues associated with these two time points that limited our analysis to the 6 h time point. Specifically, at 2 h, there seemed to be relatively little anti-m3D175 and 136kf α-spectrin staining, and at 10

h there seemed to be a large amount of extravasation of the TR-dextran into the surrounding brain tissue, such that the entirety of the coronal section seemed to have a reddish hue. This complicated the detection of the secondary antibody (alexa 546). Because of these complications we limited our study of cell viability with PI, anti-m3D175 and 136kf calpain cleaved α-spectrin to the 6 h time point.

2.7. Statistical analysis

All data are shown as mean ± SEM. Statistical analyses were performed using unpaired, two-tailed Student's *t* test, one-way ANOVA with Bonferroni's *post hoc* test, or two-way ANOVA with GraphPad Prism (version 4.0; GraphPad Software, San Diego, CA). $^{*}p < 0.05$, $^{**}p < 0.01$, and $^{***}p < 0.001$.

III. CHAPTER 3: RESULTS[1]

3.1. A model for examining the spatial relationship between local blood flow and ischemic damage to layer 5 neurons

Using rose bengal (RB) induced photothrombosis (Watson et al., 1985) we were able to produce stable clots in YFP expressing transgenic mice which were readily observed *in vivo* and lasted for up to 10 h as confirmed by subsequent histology. 2-photon imaging revealed that clots were associated with the deterioration of apical tuft dendritic structure 2 h after stroke (Fig. 3-1*A-A'*). Coronal sections of fixed tissue obtained from animals perfused after *in vivo* imaging sessions revealed trapping of texas red (TR)-dextran within the ischemic vessels (Fig. 3-1*B*). In each experiment RB-induced clots spanned all cortical layers and generally extended to the corpus collosum found at depths of ~900 μm. In previous studies RB was used to make local clots using laser activation of select vessels; however, here we have used an arc lamp and a relatively large area of photoactivation (~0.5 mm^2) to ensure a high degree of clotting, reducing possibility for collateral paths of blood flow (Schaffer et al., 2006). The lateral spread of clots throughout the sensorimotor cortex was on average 891 ± 181 μm (n= 2) at 2 h, 1017 ± 73 μm (n= 3) at 6 h, and 1987 ± 207 μm (n= 3) at 10 h after stroke. Clots ended abruptly with a sharp border at all time points (data not shown). Using the trapped TR-dextran as a map of the ischemic zone we could assess the spatial relationship between morphological damage to layer 5 cortical neurons and RB-induced clots throughout all layers of the cortex (Fig. 3-1*C*).

[1] A version of part of this chapter has been accepted for publication with minor revisions in The Journal of Cerebral Blood Flow and Metabolism (2006) Enright LE, Zhang S, Muprhy TH. Fine mapping of the spatial relationship between acute ischemia and and dendritic structure indicates selective vulnerability of layer V neuronal dendritic tufts within single neurons *in vivo*

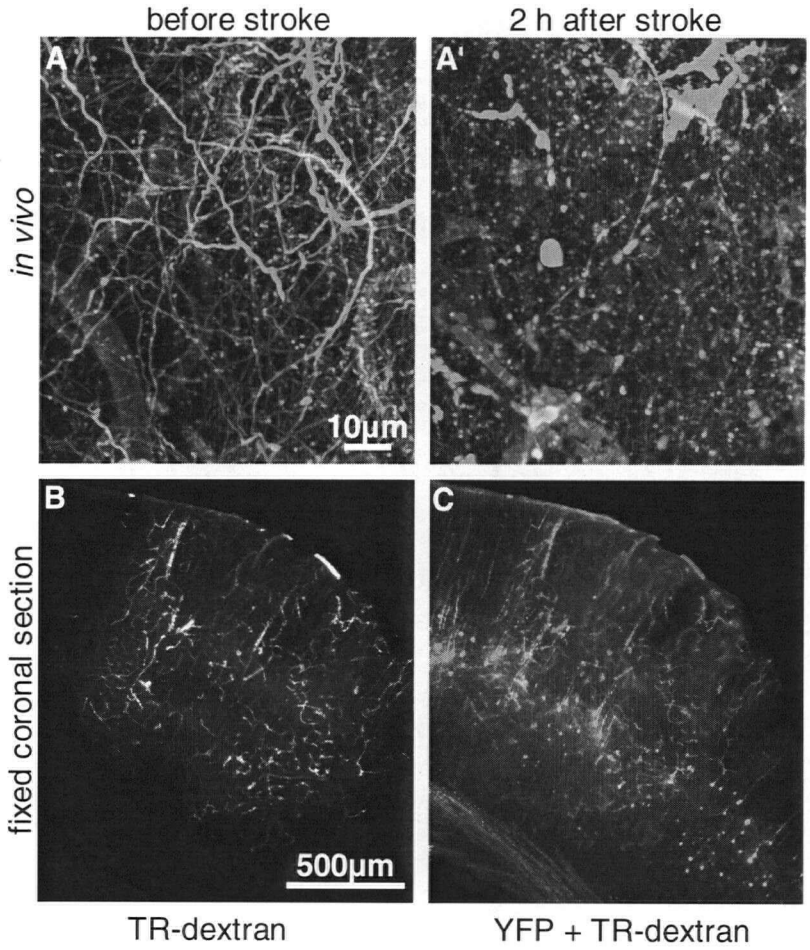

Figure 3-1. A model for examining the spatial relationship between local blood flow and ischemic damage to layer 5 neuron dendrites and axons.

A-A', *In vivo* maximum intensity projection of 100 planar scans acquired every 1 µm before *(A)* and after RB photoactivation *(A')*. Before stroke cortical tuft dendritic structure *(YFP signal; green)* and TR-dextran filled vessels *(red)* are intact, whereas 2 hours after stroke there is a widespread loss of dendritic structure and vessels have become occluded. ***B,*** Coronal section of a YFP transgenic mouse perfused 6 h after stroke and *in vivo* imaging. TR-dextran used to measure blood flow *in vivo* is caught within ischemic vessels after perfusion. ***C,*** TR-dextran *(red)* merged with YFP *(green)* signal creates a map to examine the fine spatial relationship between cortical ischemia and the resulting damage to layer 5 neurons. TR, texas-red; YFP, yellow fluorescent protein.

3.2. Laminar distribution of ischemic damage to dendrites

Given the restricted nature of RB-induced clots we were able to examine the spatial relationship between vascular clotting and neuronal damage. As expected, we found that regions with high densities of clots at the core of photoactivation showed nearly a complete loss of layer 5 neuron dendritic structure and YFP fluorescence (Fig. 3-2*A, asterisk*). In contrast, damage to neurons located near the margins of the stroke seemed to be quite localized to the dendritic tuft. To verify this apparent laminar distribution of ischemic damage to dendrites we reconstructed the entire dendritic structure from the pial surface to the cell body with 0.143 μm/pixel using high resolution confocal imaging. Specifically, we addressed whether damage to the tuft dendrites would lead to propagating damage throughout other compartments of the same neuron. In each animal 2 h (n= 2), 6 h (n= 3), and 10 h (n= 3) after stroke we examined 5-6 different cells near the ischemic interface (defined as the border where clotted vessels end) and observed the same laminar distribution of ischemic damage in each case. Specifically, we observed intense blebbing within the tuft dendrites and a complete loss of dendritic spines (Fig. 3-2*B, panel a*). Moving down the dendritic tree, the distal region (in cortical layer 2) and proximal region of the apical dendrite (spanning cortical layers 3-4) seemed to be relatively intact as indicated by the presence of spines within these regions (Fig. 3-2*B, panel b-e*). The most proximal region of the apical dendrite as it extended from the cell body also appeared to be intact although, here, spines were difficult to resolve (Fig. 3-2*B, panel f*). Since this was also observed in images of control dendrites on the opposite non-ischemic hemisphere (data not shown) this may be related to the out of focus fluorescence from the large promixal dendrite obscuring small spines. This data suggests that in neurons bordering a region of ischemia, it is possible for fine dendritic structures located in deeper cortical layers to escape ischemic damage even when the more superficial regions of these dendrites have been compromised.

One potential concern with the RB stroke model is that ischemia may be more intense within surface vessels since the photoactivation would be strongest here. Interestingly, our results argue against this and show that clots are present even 1 mm below the cortical surface. This indicates that surface photoactivation spreads clotting to deeper layers and thus dendrites in deeper layers are still ischemic, but apparently less susceptible to structural damage. To further address this point we have used a second model of stroke, the MCAO model, which does not employ photoactivation and produces ischemia throughout all cortical layers as well as in the striatum (Carmichael, 2005). A total of 3 YFP expressing mice underwent this procedure and examination of layer 5 neurons in these animals revealed a profound pattern of laminar ischemic damage in each case. As shown in Figure 3-2*C*, there was severe blebbing within the cortical tuft dendrites and distal portion of the apical dendrites (spanning cortical layers 2-3) of these neurons, but the proximal region of their apical dendrites (spanning layers 4-5) appeared to be intact. Importantly, all 3 animals also exhibited signs of subcortical striatal damage suggesting that all cortical layers were ischemic. The observation that the same pattern of ischemic damage to dendrites of layer 5 neurons was found in two separate models if ischemia strengthens the validity of our findings and suggests that dendrites in more superficial layers of the cortex are more vulnerable to ischemic damage. Although the MCAO model was perhaps more physiologically relevant, it was extremely difficult to perform and only variable levels of reperfusion were produced. We also found that the MCAO model did not result in significant trapped TR-dextran since a small degree of blood flow returned upon suture removal permitting the TR-dextran to be washed out during perfusion. Given the advantages of the RB model, such as localized clotting and trapping of TR-dextran to map ischemic zones, we continued to use it for all subsequent analysis.

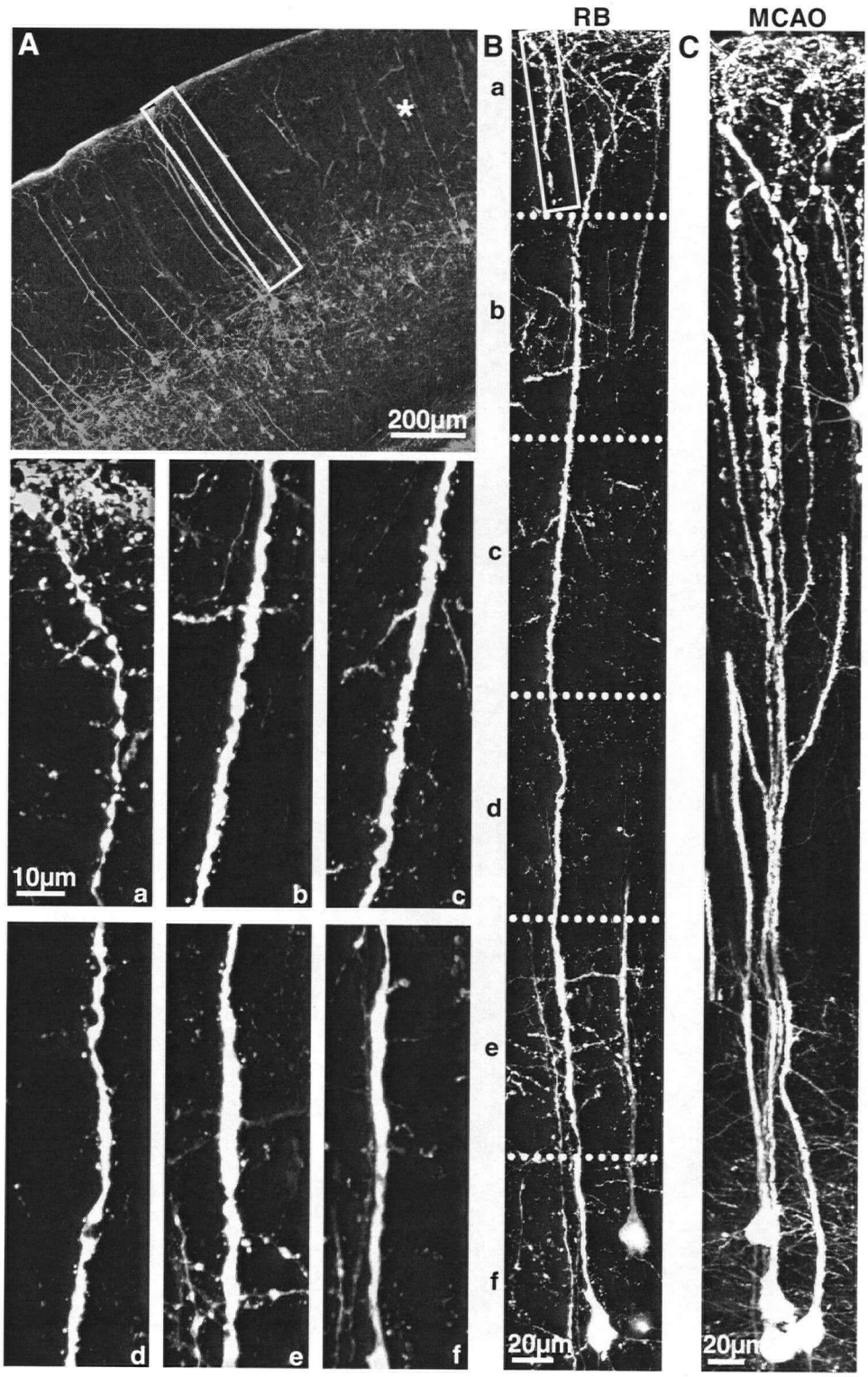

Figure 3-2. Neurons located at the ischemic border show a laminar distribution of ischemic dendritic damage.

A, Tiled confocal image of a coronal section of a YFP expressing transgenic mouse 6 h after RB-induced stroke. Ischemic vessels are those with TR-dextran caught within them *(red).* Neurons located at the core of ischemia show nearly a complete loss of YFP fluorescence and dendritic structure *(asterix, *),* whereas damage to neurons located near the border of the ischemic zone is most prominent within the dendritic tuft. The box shows the neuron in *B.* ***B,*** Reconstructed confocal image of a YFP expressing layer 5 cortical neuron. The box demarks the dendrite shown in *panel a.* ***panels a-f,*** Enlarged segments of the dendrite in *B.* The dendritic tuft is largely blebbed and no spines are apparent *(a),* however the rest of the dendrite appears to be intact, with visible spines *(b-e).* Note that the most proximal region of the apical dendrite is still intact even though there are no visible spines in this region *(f).* This was also observed in images of control dendrites on the non-ischemic hemisphere and is thought to be related to very strong out of focus fluorescence from the large promixal dendrite obscuring small spines. ***C,*** Reconstruction of a YFP expressing layer 5 cortical neuron after the MCAO stroke model. Similarly to the RB model, the dendritic tuft is severely blebbed but the more proximal region of the apical dendrite appears to be intact. RB, rose bengal; MCAO, middle cerebral artery occlusion

3.3. Spatial distribution of ischemic damage to dendrites

Stroke is characterized by a region of complete cell death at the core of the lesion with adjacent regions of partial ischemic damage (Katsman et al., 2003). It is within these regions of peri-infarct cortex that neuronal plasticity and repair after stroke have been shown to occur (Carmichael, 2003). We wished to determine the extent of ischemic damage to dendrites beyond the stroke core as well as the time course of this damage in order to establish how much of peri-infarct circuitry is potentially salvageable and thus may contribute to recovery acutely after stroke. Using TR-dextran labeled fluorescent clots as a means of identifying ischemic zones we determined how far laterally dendritic damage would spread throughout the cortex from areas with clotted blood vessels at 2 h, 6 h, and 10 h after stroke. First, we performed a low-resolution

analysis by scoring dendrites as being beaded or intact. A beaded dendrite was defined as an apical dendritic shaft with 2 or more periodic dendritic constrictions resembling beads on a string. No beaded dendrites were found at any time point within the non-ischemic hemisphere (n= 2 animals at 2 h, and n= 3 animals at 6 h and 10 h) or within control sham stroke animals (n= 4, subjected to 6 h of imaging) (data not shown) and all dendrites located within the ischemic core were found to be beaded at 2 h (Fig. 3-3*A*), 6 h (Fig. 3-3*B*), and 10 h (Fig. 3-3*C*) after stroke. In order to determine if dendritic damage changed as a function of time and distance from the infarct, we performed a 2-way analysis of variance (ANOVA) with time and distance as factors. Our analysis revealed that there was a significant effect of distance ($F_{5, 30}$= 49.33; $p<0.001$) as well as time after stroke ($F_{2, 30}$= 12.93, $p<0.001$) on the extent of beaded dendrites; however, no significant interaction was observed between these two variables ($F_{10, 30}$= 0.87, p= 0.57) (Fig. 3-3*D*). For each time point, we pooled data at all distances together and found that dendritic damage increased significantly from 2 h (10.0% ±1.7%, n= 2) to 6 h (37.3 ± 6.2%, n= 3) (t= 3.39, $p<0.05$; unpaired t-test), but did not increase further at 10 h after stroke (42.4% ± 5.9%) (p= 0.59; unpaired t-test) (Fig. 3-3*E*). For each distance, we pooled data at all time points together and found that dendritic damage decreased with distance from the ischemic interface (Fig. 3-3*F*). Specifically, there was nearly a 50% decrease in the number of beaded dendrites between 0 μm (100% ± 0, n= 8) and 100 μm (54.4 ± 6.5%, n= 8) away from the ischemic interface. There was also a significant decrease in the number of beaded dendrites between 100 μm (54.4 ± 6.5%, n= 8) and 200 μm (35.6% ± 6.8%) away from the ischemic interface (t= 2.5, $p<0.05$; unpaired t-test). This analysis indicates that the incidence of beaded and hence damaged dendrites falls sharply with increasing distance from the ischemic interface and increases with time after stroke, up to 6 h but not thereafter.

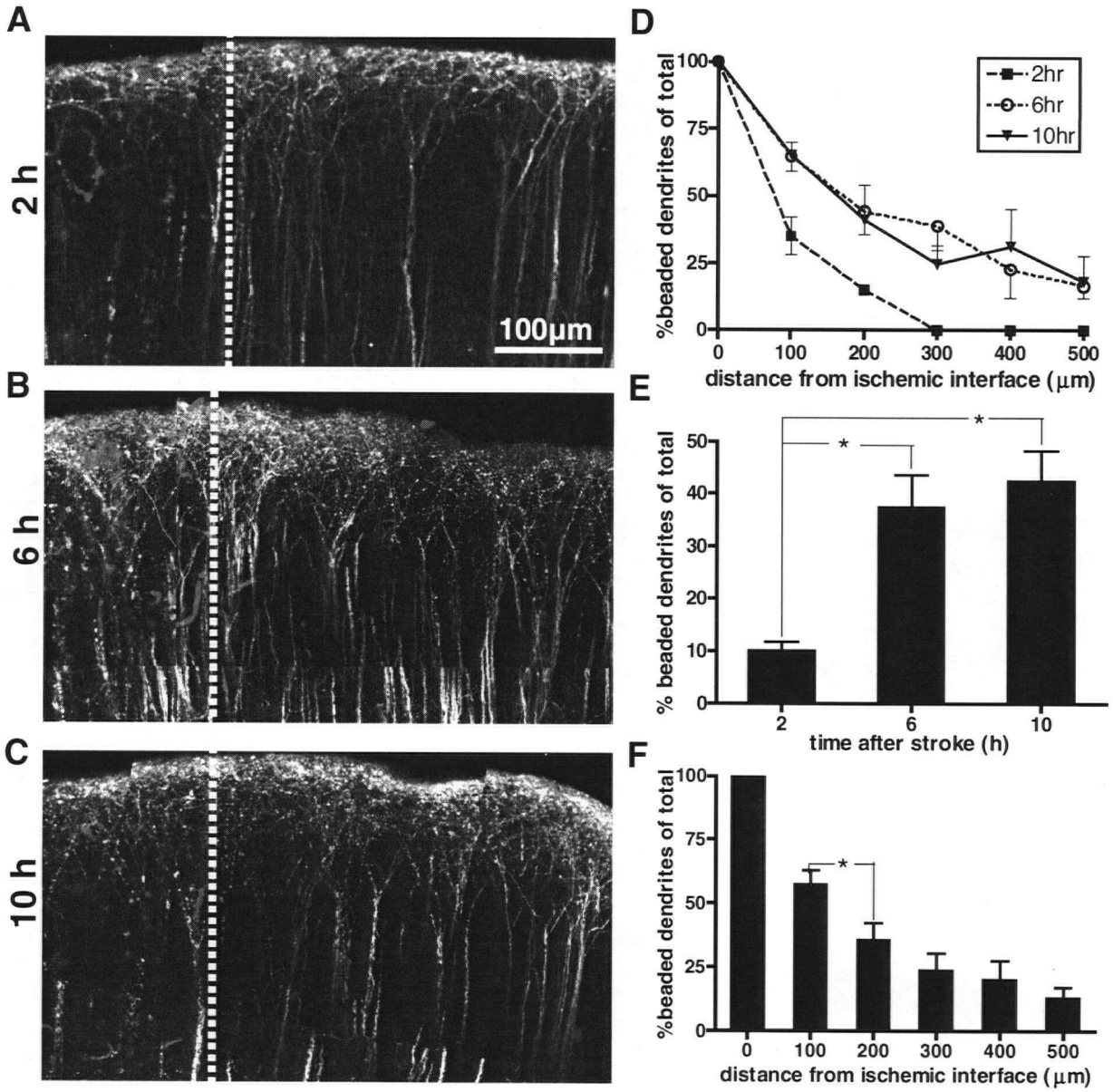

Figure 3-3. Spatial distribution of ischemic damage to dendrites.

A-C, Tiled images of coronal sections of YFP mice displaying the border of the ischemic lesion *(dashed line)*, 2 h *(A)*, 6 h *(B)* and 10 h *(C)* after RB-induced stroke. ***D,*** Dendritic damage as assessed by beading in the distal portion of the apical dendrite varies as a factor of time ($p < 0.001$) and distance ($p < 0.001$) from the ischemic interface but there is no interaction between these two factors (2-way ANOVA). There were no beaded dendrites found within the non-ischemic hemisphere of animals 2 h, 6 h, or 10 h after

stroke or in sham stroke controls (n= 4 animals). ***E,*** The percentage of YFP layer 5 neurons with beaded dendrites within 500 μm of the ischemic zone increases from 2 h to 6 h after stroke from but does not increase further at 10h after stroke (0-500 μm data pooled). ***F,*** Dendritic damage decreases with increasing distance from the ischemic interface (2 h, 6 h, and 10 h data pooled). There is nearly a 50% decrease in cells with beaded dendrites found within the first 100 μm from the ischemic interface and there is also a significant decrease in beading from 100 μm to 200 μm. Data represent mean ± SEM collected from n=2 animals at 2h, and n=3 animals at 6 h and 10 h. $p < 0.05$ (*); unpaired t-test.

To verify that certain neurons located as close as 100 μm from the stroke core could be entirely free of ischemic damage we also performed a high-resolution analysis of 5-6 non-beaded layer 5 YFP neurons located between 100 and 300 μm from the ischemic interface at 2 h (n= 2), 6 h (n= 3) (Fig. 4-4*A*), and 10 h (n= 3) after stroke. Using confocal imaging, we reconstructed the entire dendritic structure of these neurons, from the cell body to the cortical tuft dendrites (Fig. 3-4*B*). This analysis revealed that the spines and dendritic structure of these neurons could be intact throughout all cortical layers (Fig. 3-4*B*, *panels a-f*), including the most superficial dendritic tuft (Fig 3-4*B*, *panel a*). Thus, layer 5 neurons located at the ischemic interface show a laminar distribution of dendritic damage, whereas those as close as 100 μm from the lesion can retain structural integrity throughout their length.

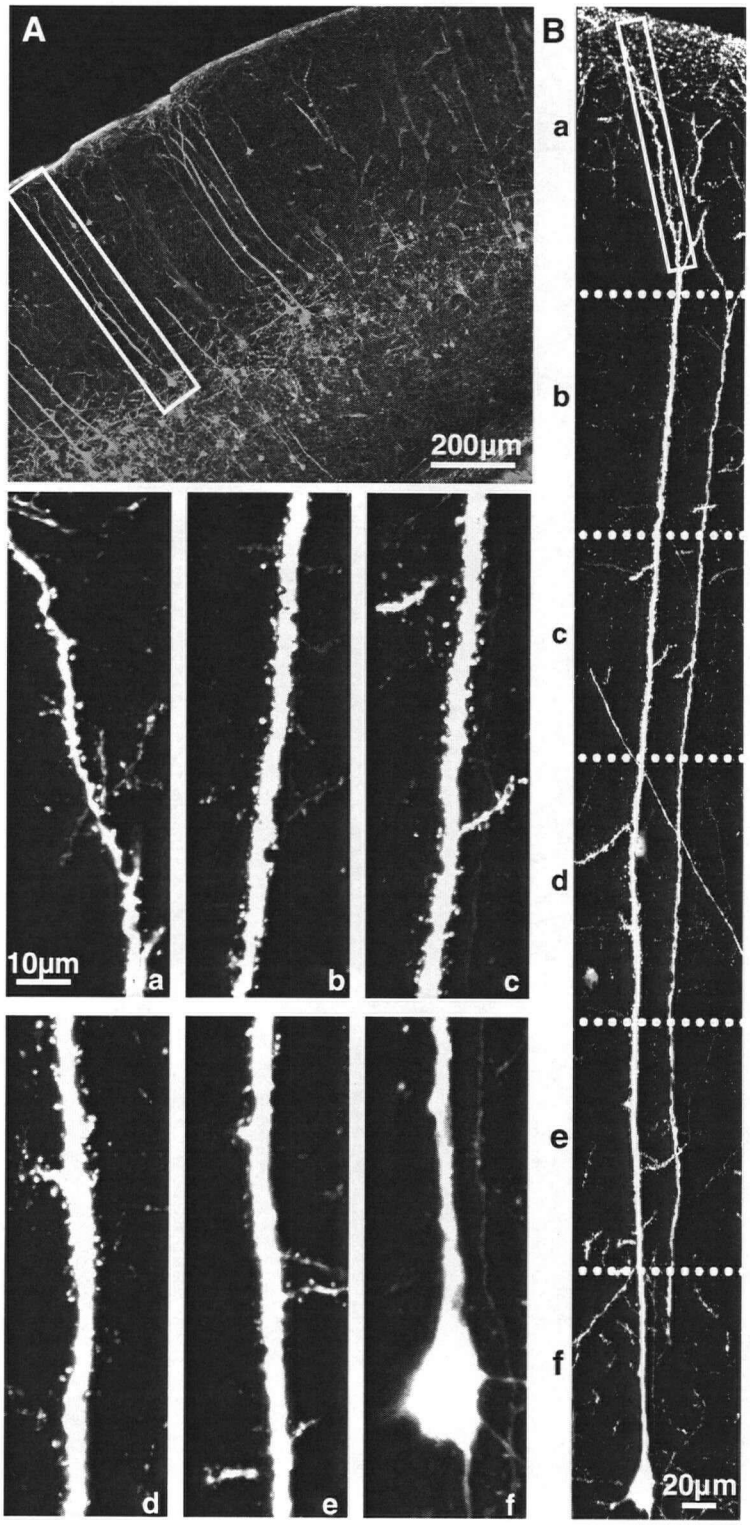

Figure 3-4. Neurons located near a region of ischemia region show intact dendritic structure throughout their length.

A, Tiled confocal image of a coronal section of a YFP expressing transgenic mouse 6 h after stroke showing TR-dextran filled ischemic vessels *(red)*. The box denotes the neuron in *B*. ***B,*** Reconstructed confocal image of a YFP expressing layer 5 cortical neuron. The box outlines the denrite shown in *panel a*. ***panels a-f,*** Enlarged segments of the dendrite in *B* shows that it is intact throughout its length. Spines may be resolved on the dendrite at all levels *(a-e)* with the exception of the most proximal region of the dendrite extending from the cell body *(f)*.

3.4. Spatial distribution of ischemic damage to axons

The extent of axonal ischemic damage was also of interest as layer 5 cortical neurons are the major output neurons of the cortex that synapse within the midbrain, hindbrain, and spinal cord, ultimately affecting motor function (O'Leary and Koester, 1993). Further, as we found there to be a graded spatial and temporal distribution of ischemic damage to the dendrites of these neurons we were interested to uncover whether these factors would have similar effects on their axons. Axonal beading has previously been shown to be a response to anoxic (Tekkok et al., 2005) and oxidative damage *in vitro* (Roediger and Armati, 2003) that could accompany ischemia/reperfusion during the RB model (Zhang et al., 2005). Thus, we used this morphological characteristic as a representation of axonal ischemic damage. The control animals (n= 4) were those which received a sham stroke where a craniotomy was made and animals were subjected to laser exposure with no injection of RB dye, but 6 h of imaging. A very moderate level of axonal damage was apparent in these controls within a similar region to animals that underwent RB photoactivation (Fig. 3-5*A*). This slight apparent damage in the control group varied somewhat across the medial to lateral extent of the brain and was possibly associated with

mechanical effects of the craniotomy or its impact on the perfusion/brain removal process. In animals that received a RB stroke, observation of the axons of layer 5 neurons within the ischemic core and adjacent cortex revealed that beaded axons were located well beyond the ischemic interface and that this effect became more apparent with time after the stroke (Fig. 3-5*B-D*). To further elucidate the extent of axonal damage throughout space and time in both stroke animals and sham controls we devised an axonal damage rating (ADR) scale where 0= no axonal damage (all dendrites intact), 1= minor damage (~25% of axons beaded), 2= moderate damage (~50% of axons beaded), and 3= severe damage (~75% of axons beaded or complete loss of axonal integrity) (Fig. 2-1). In order to determine if axonal damage varied as a function of time and distance from the ischemic infarct we performed a 2-way ANOVA with time and distance as factors. Our analysis revealed that there was a significant effect of distance from the ischemic interface ($F_{7, 32}$= 5.35, $p<0.001$) as well as time after stroke ($F_{2, 32}$= 6.61, $p<0.01$) on the level of axonal damage but there was no interaction between these two variables ($F_{14, 32}$= 0.20, p= 0.99) (Fig. 3-5*E*). For each time point, we pooled the ADR scores at all distances together and found that when compared to sham control values the level of axonal damage was increased at 2 h (1.53 ± 0.47, n= 2) but not significantly (t=2.6, p=0.06; unpaired t-test), and significantly increased at 6 h (1.88 ± 0.40, n= 3) (t= 3.5, $p<0.05$; unpaired t-test) and at 10 h (2.55 ± 0.24, n= 2) (t= 6.4, $p<0.01$; unpaired t-test) after stroke (Fig. 3-5*F*). Although there was a trend towards increasing damage with time after stroke, this effect was not considered to be statistically significant (between 2, 6, and 10 h). For every distance we also pooled together the ADR scores from each time point and found that the level of axonal damage was significantly greater than sham control values from 100-600 μm beyond the ischemic interface but dropped to near control levels at 700 μm (Fig. 5*G*). The level of axonal damage at 700 μm (1.10 ± 0.30, n= 7) and 800 μm (0.85 ± 0.26, n= 7) away from the ischemic interface did not differ significantly from sham control values (700 μm: 0.75 ± 0.29; 800 μm: 0.50 ± 0.22; n= 4) (700 μm: t=0.75, p=0.47; 800

μm: t= 0.86, p= 0.41; unpaired t-test). Thus it seems that the spatial spread of axonal damage increases with time after stroke and extends further laterally throughout the cortex than does ischemic damage to dendrites. This suggests that the axons of layer 5 neurons may be more vulnerable to ischemia than their dendrites.

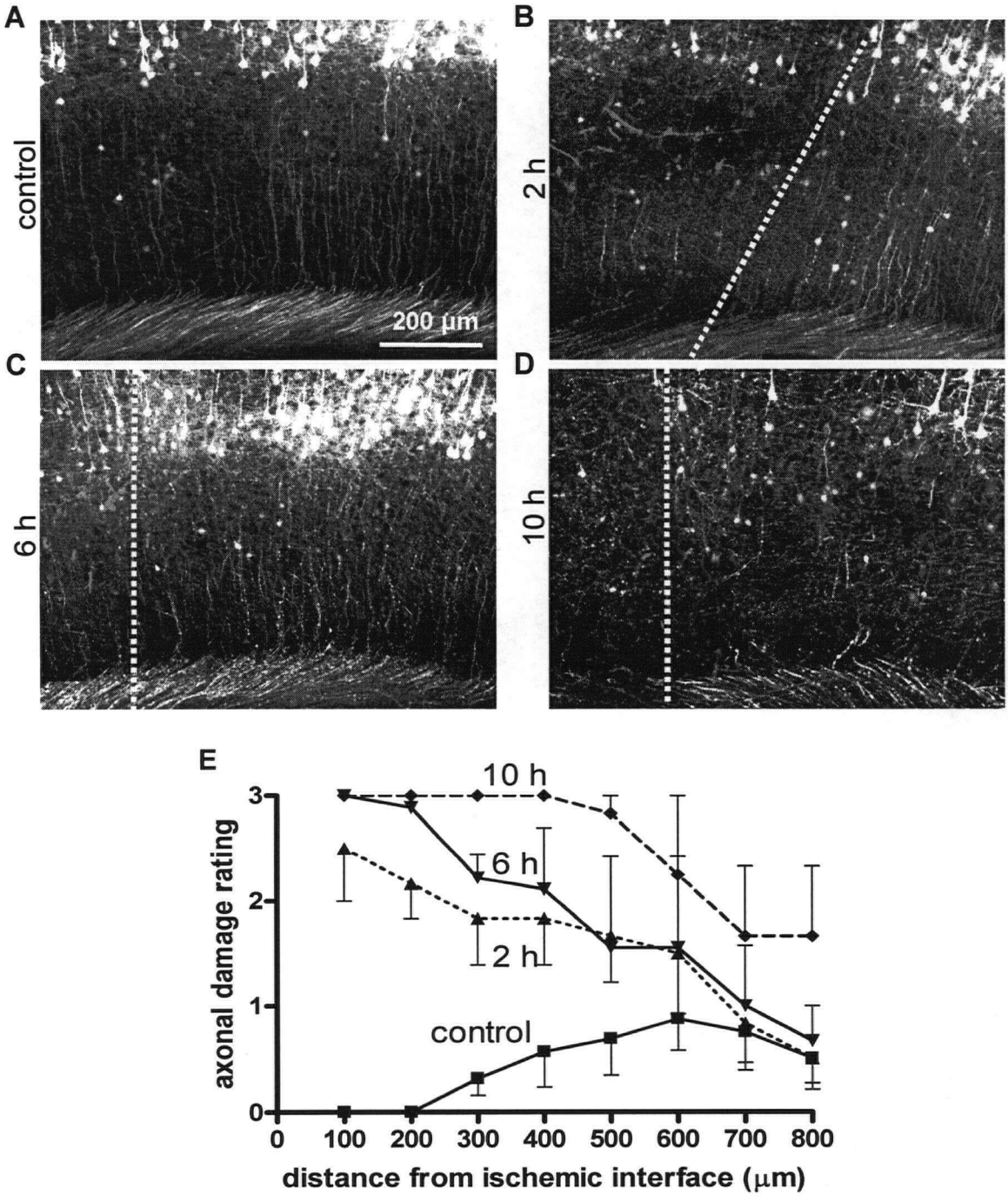

Figure 3-5. Spatial distribution of ischemic damage to axons.

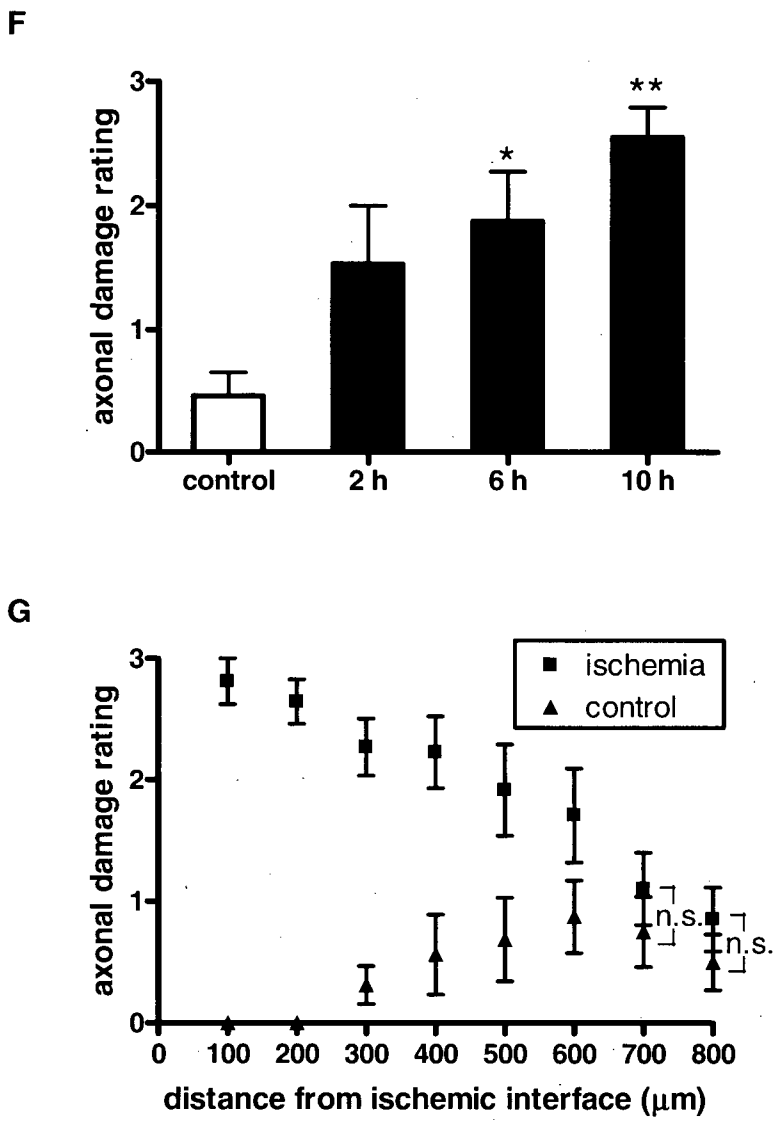

Figure 3-5. Spatial distribution of ischemic damage to axons.

A-D, Coronal sections of YFP transgenic mice with a sham stroke operation *(control, A)* and 2h *(B)*, 6h *(C)* and 10h *(D)* after stroke showing ischemic vessels (red) and axons of layer 5 cortical neurons. Axonal damage (beading) extends beyond the ischemic interface (dashed line) at all time points after stroke and the level of axonal damage increases notably with time *(B-D)*. ***E,*** Axonal damage varies as a factor of time ($p<0.01$) and distance ($p<0.001$) from the ischemic interface, but there is no interaction between

damage was apparent in lateral regions of control animals. This may have been related to the mechanical effects of the craniotomy or its impact on the perfusion process. ***F,*** The level of axonal damage increases significantly at 6 h and 10 h after stroke (versus control) but no statistically significant differences were observed between 2 h, 6 h, and 10 h time points. ***G,*** Axonal damage extends well beyond the ischemic interface and does not drop to near control values until 700 μm from the ischemic interface. Data represent mean ± SEM collected from n=2 animals at 2 h and 10 h, and n=3 at 6 h. $p < 0.05$ (*), $p< 0.01$ (**) versus control; unpaired t-test.

3.5. Cell fate throughout the ischemic core and penumbra

Focal dendritic swelling or beading is a typical response of neurons to hypoxic and excitotoxic conditions (Majno and Joris, 1995; Andrew et al., 1999; Jarvis et al., 1999; Hasbani et al., 2001). Here, we have been using axonal and dendritic beading as a measure of compromised neuronal circuitry; however, it is not entirely clear what the fate is of neurons exhibiting this type of beaded morphology. In order to determine the viability of layer 5 neurons located throughout the ischemic core and penumbra 6 h after stroke we first used propidium iodide (PI) staining to assess the integrity of cells' nuclei by measuring their size. PI is generally used as a marker of cell death in cell culture and live tissue slices because, in these cases, it stains only cells with a compromised plasma membrane. Here, because we used PI staining on fixed and permeabilized tissue slices all cells were labeled with PI, thus we chose to use the size of a cell's nucleus as a measure of its integrity. An analysis of only YFP expressing layer 5 neurons within the non-ischemic hemisphere (control; Fig. 3-6*A-A'*), stroke core (-150-0 μm; Fig 3-6*B-B'*), as well as 0-150 μm, 150-300 μm and 300-450 μm (Fig. 3-6*C-C'*) away from the ischemic interface (defined as 0 μm) revealed that distance from the ischemic interface had a significant effect on the size of a cell's nucleus ($p<0.001$; ANOVA). More specifically, the

nucleus size of YFP cells located within the stroke core (83.5 ± 5.9 μm^2, n= 3 animals) as well as 0-150 μm (68.3 ± 4.1 μm^2, n= 3 animals) and 150-300 μm (76.2 ± 6.3 μm^2, n= 3 animals) away from the ischemic interface was significantly smaller than that of control YFP cells (143.1 ± 3.0 μm^2, n= 4 animals) ($p<0.001$; ANOVA with Bonferroni's *post-hoc* test) (Fig. 3-6*D*). Interestingly, the nuclei of YFP cells located between 300-450 μm away from the edge of the ischemic zone (121.6 ± 7.7 μm^2, n= 3 animals) were significantly larger than the nuclei of cells located between 150-300 μm away ($p<0.01$; ANOVA with Bonferroni's *post-hoc* test) and not statistically different from control YFP cells ($p>0.05$; ANOVA with Bonferroni's *post-hoc* test) (Fig. 3-6*D*). Thus it seems that cells located up to 300 μm from the border of the ischemic zone are compromised, as indicated by the condensed size of their nucleus, whereas cells beyond this distance are relatively intact. This could indicate a penumbral zone where cells may be functionally impaired but potentially still viable.

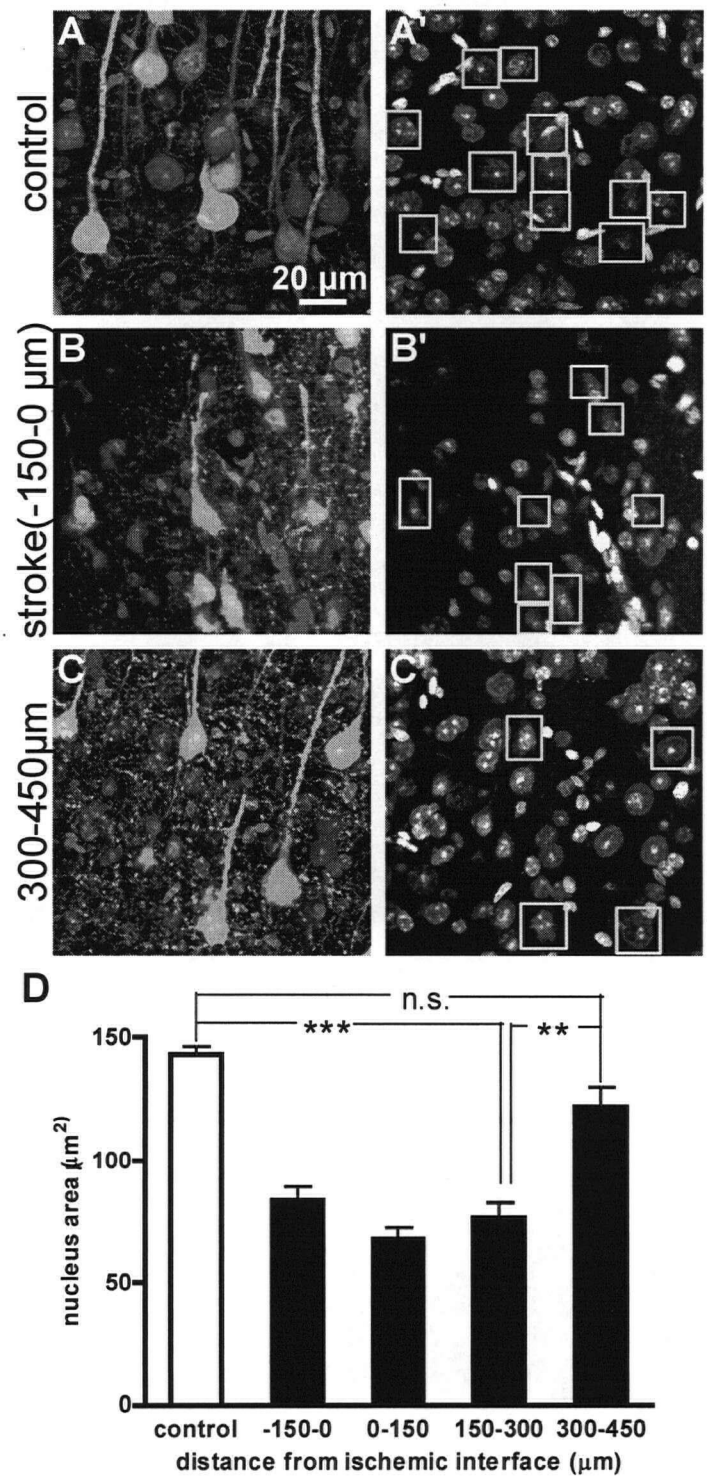

Figure 3-6. PI staining reveals changes in nuclear size of YFP layer 5 neurons throughout the ischemic core and penumbra.

A-C, High resolution confocal images of layer 5 cortical neuron cell bodies (green) from a YFP transgenic mouse 6 h after stroke. Cells were imaged in 150 μm bins within the contralateral non-ischemic hemisphere *(control; A),* the stroke core *(-150-0 μm; B)* and the ischemic penumbra (0-150 μm, 150-300 μm and 300-450 μm) *(300-450 μm; C).* The nuclei of all cells have been labeled by PI (red) and therefore many non-YFP expressing cells are seen. ***A'-C',*** PI labeling channel only with the nuclei of YFP cells denoted in boxes (note PI stains the nucleus of all cells). The nuclei of control YFP cells are round *(A')*; whereas, the nuclei of YFP cells within the stroke core are condensed *(B').* YFP cells located between 300-450 μm away from the edge of ischemia are nearly as large and round as those within the non-ischemic hemisphere *(C').* ***D,*** The nuclei of YFP cells located within the stroke core (-150-0 μm) and up to 300 μm away from the ischemic interface are significantly smaller than the nuclei of control YFP cells. The nuclei of YFP cells located beyond 300 μm from the ischemic interface are significantly larger than cells between 150-300 μm and not statistically different than control cells. The data represent mean ± SEM collected from n=3 animals at 6 h after stroke. $p < 0.01$(**); $p < 0.001$ (***), ANOVA with Bonferroni's post-hoc test.

3.6. Spatial profile of neuronal apoptosis in the ischemic core and penumbra

As nuclear condensation is a morphological characteristic of apoptosis (Majno and Joris, 1995), is it probable that cells with condensed nuclei may be undergoing this form of cell death. To examine this possibility we performed immunostaining on sections of YFP mice 6 h after stroke using antiserum against the caspase-3 cleavage site (Urase et al., 2003) (Fig. 3-7*A*). Caspase-3 is a cytosolic cysteine protease whose activation has been shown to be associated with apoptotic cell death after ischemic brain injury (Chen et al., 1998; Namura et al., 1998). Indeed, we found many layer 5 YFP neurons within the stroke core (Fig. 3-7*B, panel 1*) as well as in the ischemic penumbra (Fig. 3-7*B, panels 2-3*) to be anti-m3D175 positive; however, there was

significantly less staining in YFP neurons located between 300-450 μm away from the stroke border (Fig. 3-7*B, panel 4*). YFP neurons located on the non-ischemic hemisphere did not show any anti-m3D175 staining indicating specificity of the antibody (Fig. 3-7*B, panel ctrl*). Analysis of the number of anti-m3D175 positive YFP apoptotic cells with distance from the ischemic interface revealed a similar spatial distribution to cells with condensed nuclei as indicated by PI staining (Fig. 3-7*C*). Specifically, the number of anti-m3D175 positive apoptotic YFP neurons located within the stroke core (-150-0 μm; 84.2 ± 4.1%) did not differ significantly from those located between 0-150 μm (77.9 ± 5.0%) or 150-300 μm (82.9 ± 2.7%) in the ischemic penumbra, ($p>0.05$; ANOVA with Bonferroni's *post-hoc* test; n= 3 animals). Beyond this distance, between 300-450 μm, significantly fewer YFP neurons were labeled with anti-m3D175 (24.9 ± 7.8%) ($p<0.001$; ANOVA with Bonferroni's *post-hoc* test). Thus neuronal apoptosis appears to be activated 6 h after stroke within the core of the ischemic lesion and extending up to 300 μm in the surrounding penumbral tissue.

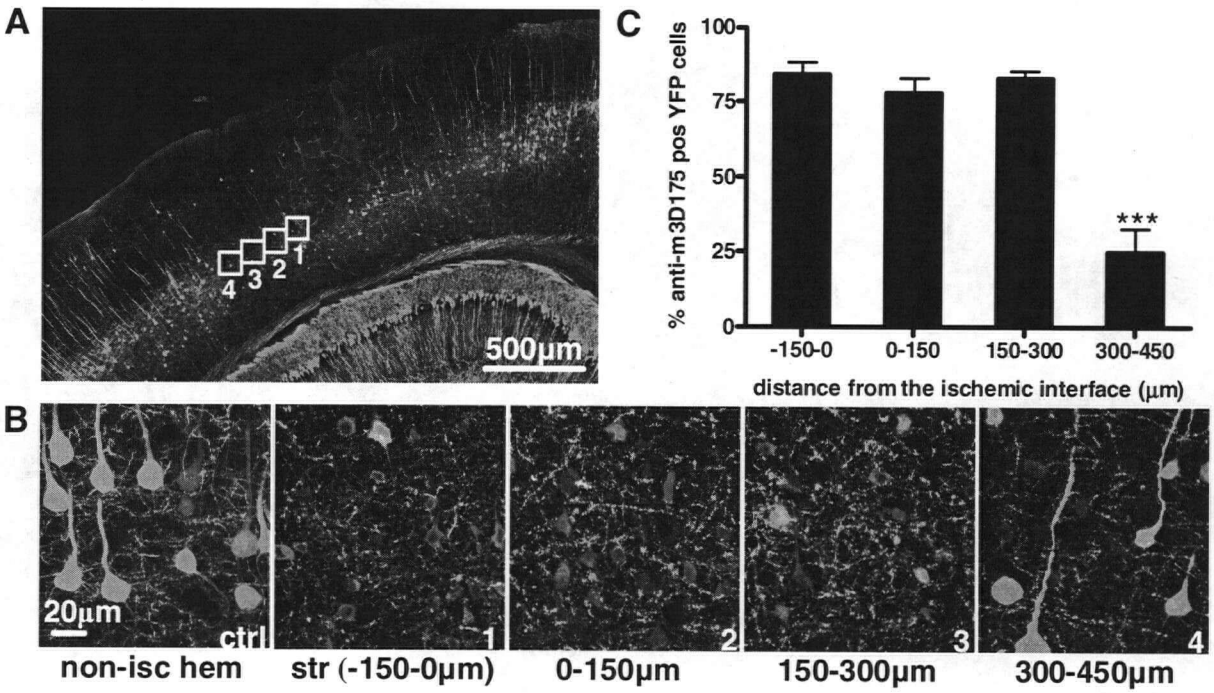

Figure 3-7. Spatial pattern of neuronal apoptosis 6 h after RB stroke.

A, Coronal section of a YFP expressing transgenic mouse depicting ischemic vessels by trapped TR-dextran (red) 6 h after RB stroke. Boxes 1-4 show 150 µm bins (in *B*) throughout the stroke core and penumbra that were imaged at high resolution. ***B,*** High power confocal images of activated apoptotic cell death indicated by immunostaining against the caspase-3 cleavage, anti-m3D175 (red). There are no apoptotic cells within the contralateral non-ischemic hemisphere *(ctrl).* Most YFP neurons within the stroke core *(box 1)* and up to 300µm away from the ischemic interface *(box 2,3)* are apoptotic. Beyond 300 µm from the ischemic border, fewer YFP cells are apoptotic *(box 4).* ***C,*** There was a similar elevated level of anti-m3D175 positive apoptotic YFP cells within the stroke core and up to 300µm away from the edge of ischemia. Beyond this distance the number of anti-m3D175 postitive apoptotic YFP cells was significantly reduced. Data represent mean ± SEM collected from n=3 animals at 6 h after stroke. $p<0.001$ (***); ANOVA with Bonferroni's post-hoc test. ctrl, control; non-isc hem, non-ischemic hemisphere; str, stroke; pos, positive

3.7. Spatial profile of neuronal necrosis in the ischemic core and penumbra

Both apoptotic and necrotic cell death cascades have been implicated in ischemia (Yamashima, 2004) and these have been shown to be concomitantly activated in the same set of ischemic neurons (Unal-Cevik et al., 2004). We wished to determine if and where necrotic cell death cascades were occurring in our animals, 6 h after stroke. To test this, we performed immunostaining on slices of YFP mice 6 h after stroke using an antibody to the 136-kDa fragment of calpain-cleaved α-spectrin (Fig. 3-8*A*). Calpain is a calcium-dependent neutral cysteine protease that is known to be activated after brain ischemia (Yamashima et al., 2003) and the 136-kDa fragment of calpain-mediated α-spectrin breakdown is only generated during neuronal necrosis making it a specific marker for this form of cell death (Takano et al., 2005). The spatial pattern of activated necrotic cell death indicated by staining for the 136-kDa fragment of calpain-cleaved-α-spectrin was similar to the spatial pattern of activated apoptotic cell death indicated by anti-m3D175 staining. No cells in the non-ischemic hemisphere stained for the 136kf of α-spectrin (Fig. 3-8*B, panel ctrl*); however in stroke core (-150-0 μm) nearly all YFP cells were 136kf α-spectrin positive (95.4 % ± 4.5%, n= 3 animals) (Fig. 3-8*B, panel 1*). There was a high number of 136kf α-spectrin positive YFP neurons located between 0-150 μm (94.0% ± 1.7%, n=3 animals) (Fig. 3-8*B, panel 2*) and 150-300 μm (84.3% ±11.6%, n=3 animals) (Fig. 3-8*B, panel 3*) away from the ischemic interface (denoted as 0 μm); however, between 300-450 μm this number decreased drastically to 37.4% ± 5.5% (n= 3 animals) (Fig. 3-8*B, panel 4*). The number of potentially necrotic 136 kf α-spectrin positive YFP neurons between 300-450 μm away from the ischemic interface was significantly reduced compared to those located in the core of the stroke and up to 300 μm away ($p< 0.05$; ANOVA with Bonferroni's *post-hoc* test) (Fig. 3-8*C*). Thus, it appears that necrotic and apoptotic cell death cascades are activated in a similar spatial pattern 6 h after stroke. Since the percentage of YFP cells that stained for these markers approached 90% (near the core) we would expect that

individual layer 5 neurons would have components of both cell death pathways activated within them.

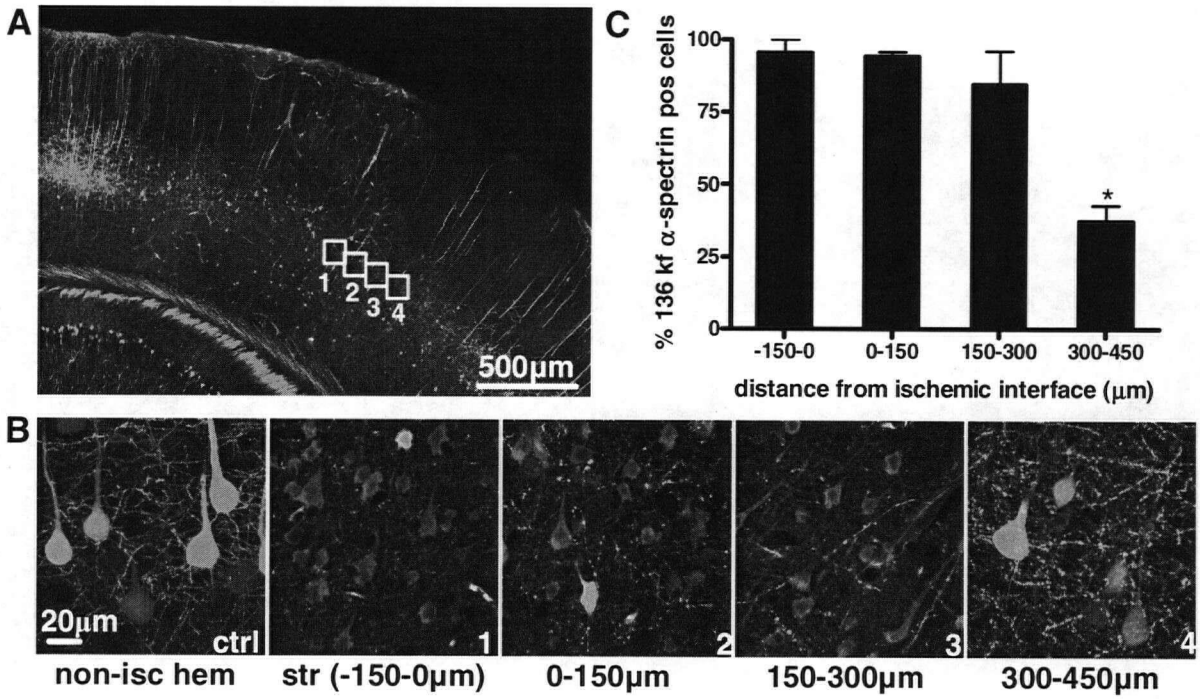

Figure 3-8. Spatial pattern of neuronal necrosis 6 h after RB stroke.

A, Spatial map showing the location of ischemic vessels by trapped TR-dextran *(red)* in a coronal section of a YFP expressing transgenic mouse 6 h after stroke. Boxes 1-4 denote 150 µm bins where high power images (in *B*) were taken. ***B,*** High power images of activated necrotic cell death indicated by immunostaining for the 136-kDa fragment of calpain-cleaved-α-spectrin in YFP neurons (red). There are no necrotic cells within the contralateral non-ischemic hemisphere *(c).* Nearly all YFP neurons within the stroke core *(box 1)* and up to 300 µm away from the edge of ischemia *(box 2,3)* are necrotic. Beyond this distance there is a significant drop in necrotic YFP neurons *(box 4).* ***C,*** There was high percentage 136kf calpain-cleaved-α-spectrin positive YFP cells located within the stroke core (-150-0 µm) and up to 300 µm away from the edge of ischemia. Beyond this distance, between 300-450 µm, calpain activation was significantly reduced. Data represent mean ± SEM collected from n=3 animals at 6 h after stroke. $p<0.05$ (*); ANOVA with Bonferroni's post-hoc test. ctrl, control; non-isc hem, non-ischemic hemisphere; str, stroke; pos, positive

IV. CHAPTER 4: DISCUSSION

4.1. A sharp border exists between normal and damaged synaptic circuitry

Rose bengal induced photothrombosis is an ideal model of stroke to study the spatial spread of ischemic damage to neurons since a well defined ischemic zone can be created by using focused light (photoactivation). The model effectively induces clots in vessels of all sizes and avoids issues associated with unblocked collateral blood vessels. Further, in the RB stroke model used here, TR-dextran was found to become lodged within ischemic vessels upon fixation providing a map of the ischemic zone.

In our study, we used RB photothombosis together with YFP fluorescence of layer 5 neurons to map the extent of axonal and dendritic damage in relation to the location of ischemia within the first 2-10 h after stroke. Dendritic beading was used as a measure of neuronal damage as this has been shown to be an early marker of excitotoxic and anoxic damage to neurons (Hori and Carpenter, 1994; Park et al., 1996; Jarvis et al., 1999). Our analysis shows that the incidence of beaded dendrites falls sharply with increasing distance from the lesion site, with nearly a 50% decrease in the number of beaded dendrites within the first 100 μm from the ischemic core border and no beaded dendrites beyond 500 μm. In another study, assessment of neuronal function in peri-infarct cortex with cytochrome oxidase (CO) staining (Wong-Riley, 1989) 7 days after focal stroke revealed that the region of partially damaged synaptic structures extended ~0.5 mm laterally and ~1.1 mm medially from the lesion edge (Katsman et al., 2003). The fact that we observed sharper ischemic borders than in this study could reflect that we examined a significantly earlier time point (2-10 h vs. 7 d) and also used more sensitive measures of aberrant synaptic structure such as spine loss and dendritic beading in contrast to CO staining that

provides a crude measure of cellular metabolism (Wong-Riley et al., 1989). In addition, we may have more precisely located the region of ischemia by using trapped texas red dextran.

Although the size of our ischemic lesions increased with time, the lateral spread of damage to dendrites remained relatively confined to the location of ischemia (~50% decrease in damage 100 μm from the ischemic interface) regardless of the time after stroke (2 h, 6 h, or 10 h), or the potential for diffusion of released cytotoxic factors such as glutamate, nitric oxide, or other factors from the dying core (Sharp et al., 2000; Witte et al., 2000). Perhaps these cytotoxic factors have a limited range of diffusion due to uptake and inactivation mechanisms and only affect cells within the stroke core. Alternatively, local resting microglia may become activated by the ischemic insult and infiltrate the site of injury, thus acting to contain ischemic damage. Recently a neuroprotective role of microglia has been supported *in vivo* by their immediate response to local damage (Davalos et al., 2005; Nimmerjahn et al., 2005). Further, these cells were shown to have spherical-shaped inclusions which suggests that they were involved in the removal of potentially damaging debris from the extracellular environment.

4.2. Selective damage to cortical tuft dendrites

From *in vivo* imaging studies in our lab it is clear that after photothrombotic stroke neuronal circuitry within the ischemic core is intensely damaged specifically at the level of the dendritic tuft (Zhang et al., 2005). Although reperfusion may be associated with the return of dendritic structure (Zhang et al., 2005), the tissue at the core of the stroke is generally considered to be irreversibly damaged and is therefore unlikely to contribute to recovery (Witte et al., 2000). In contrast, the fate of neurons and their synaptic circuitry at the margins of ischemia is unclear and is likely to be a critical determinant of functional recovery since this circuitry, by proximity, often functions in a related manner to tissue lost in the core (Camichael, 2003). Here, we wished

to uncover whether the damage to tuft dendrites after stroke monitored by *in vivo* 2-photon imaging would propagate into deeper layers of the cortex. Examination of the distribution of ischemic damage to layer 5 neurons at the border of the ischemic zone 6 h after stroke revealed that dendritic beading was most prominent within the tuft dendrites and did not spread to the distal or proximal portion of the apical dendrite (Fig. 3-2*B*). The fact this laminar distribution of ischemic damage was also apparent at 2 h and 10 h after stroke shows that this was not necessarily a reflection of a progressive process at an intermediate time point. Another potential concern was that the selective damage to cortical tuft dendrites was a factor of the photothrombotic model of stroke used in our study. Since photoactivation would be strongest at the surface of the cortex, it is possible that this would lead to more intense damage at this level of the brain. The fact that the same pattern of ischemic damage to layer 5 neurons was also found in another model of stroke, namely the MCAO model (Fig. 3-2*C*), shows that this was not an artifact of the nature of the photochemical insult and such evidence strengthens the validity of our findings.

The central nervous system seems to be especially vulnerable to excitotoxic damage and oxidative stress on account of its high rate of oxygen utilization and the fact that neuronal membranes contain a high proportion of oxidation-prone polyunsaturated fatty acids making them more susceptible to peroxidative damage (Sayre et al., 1999). Also, the brain appears to contain lower levels of molecular antioxidants such as superoxide dismutase and glutathione peroxidase (Floyd, 1999). At the level of the cerebral cortex, it has previously been shown that certain subsets of neurons, including layer 5 neurons, are particularly vulnerable to ischemic damage (Jones and Schallert, 1992); however, compartmentalized dendritic damage within individual neurons is a relatively new finding. It is known that the expression of ion channels is not necessarily uniform throughout the length of the dendrite (Hausser et al., 2000) thus the

selective vulnerability of tuft dendrites to ischemic damage could be underscored by a higher proportion of channels making them more vulnerable to excitotoxicity. Another potential explanation for this compartmentalized damage is that processes with a higher surface area to volume ratio such as small tuft dendrites and axons are not able to buffer aberrant ion fluxes as efficiently as somatic compartments and larger dendrites thus making them more susceptible to excitotoxicity. This would also explain why the axons of layer 5 neurons at the ischemic border appeared to be more damaged than nearby proximal dendrites. Yet another possibility is that beaded tuft dendrites that we observed immediately adjacent to the lesion site were branches projecting from those neurons located within the dying core; however, in many cases we have traced these dendrites and can show this is not the case.

The idea that the more distal (tuft) region of the apical dendrite of layer 5 neurons may be more vulnerable to ischemic damage is consistent with studies showing that this region undergoes a higher degree of modification than basal dendrites following denervation (Wellman and Sengelaub, 1995; Churchill et al., 2004) or in response to an aspiration-induced stroke model (Gonzalez and Kolb, 2003). However, other studies indicate that the basal and not apical dendritic arborization of surviving peri-infarct layer 5 neurons was increased after ischemia (Biernaskie and Corbett, 2001). The loss of tuft dendrites may have implications for recovery if the neuronal somata and associated basal dendrites survive. For example, one would expect cortical layer I activity to be largely absent but deeper layers could contribute to residual circuitry during recovery. We may also expect reorganization within deeper dendritic structures.

4.3. Altered cortical connectivity

The cerebral cortex is divided into 6 layers and each layer has distinctive efferent and afferent connections, an arrangement which provides an efficient means of organizing the

complex connectivity between subsets of cortical neurons (Kandel, 2000; Fig. 4-1). Layer 1 is mainly considered to be an acellular layer consisting of dendrites and axons from the other molecular layers (Kandel, 2000). Thus this layer is thought to be responsible for integrating the majority of inputs within the neocortex. Pyramidal neurons in layers 2, 3, and 5 have all been shown to have apical dendrites that terminate in layer 1 (Cauller and Connors, 1994). Layer 2/3 cells are primarily responsible for cortico-cortical connections within the cortex; whereas, layer 5 neurons project mainly to subcortical structures such as the basal ganglia, brain stem nuclei, superior colliculus and spinal cord (O'Leary and Koester, 1993).

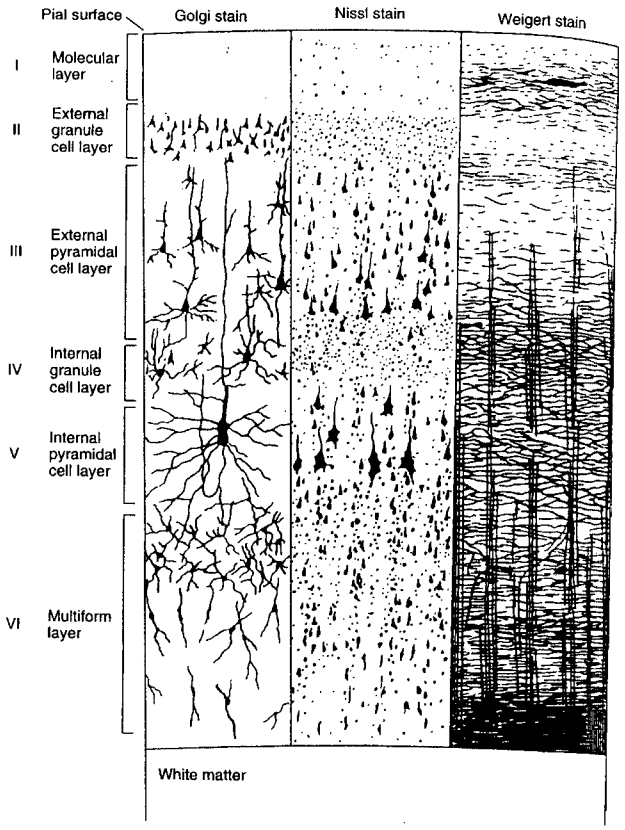

Figure 4-1. The 6 layers of the neocortex.

The neocortex is divided into 6 distinct cellular layers. Each layer may be distinguished by the morphology of the population of cells within that layer, as well as the efferent and afferent connections to those cells. Different stains reveal discrete functional components of the neurons within each layer and thus give the neocortex a unique appearance. The golgi-cox stain reveals cell somas and dendritic trees; whereas, the Nissl stain impregnates cell somas and proximal dendrites and the Weigert stain reveals the distribution of axons. (figure adapted from Kandel et al., 2000).

In our study, we noted the selective degeneration primarily of cortical tuft dendrites of layer 5 neurons. Although we were looking specifically at layer 5 neurons it is conceivable that the dendrites and axons projecting to layer 1 from neurons in other cortical layers were also severely damaged by the nearby ischemia. As layer 1 is the major source of synaptic terminations from cortico-cortical connections (Cauller and Connors, 1994) we would expect that the loss of dendritic and axonal structures within this layer would have a large impact on the neuronal signaling between associated cortical areas. One might expect this to lead to a deficit in the ability to coordinate sensation with movement, processing which is important in governing motor reflexes. Reflexes require the ability to integrate sensory feedback signals from the periphery with ongoing motor programs, and this information is conveyed by incoming afferent projections to the somatosensory cortex. Since these afferents have their primary synaptic connections within cortical layer 1, we might expect these reflexes to be selectively compromised after stroke.

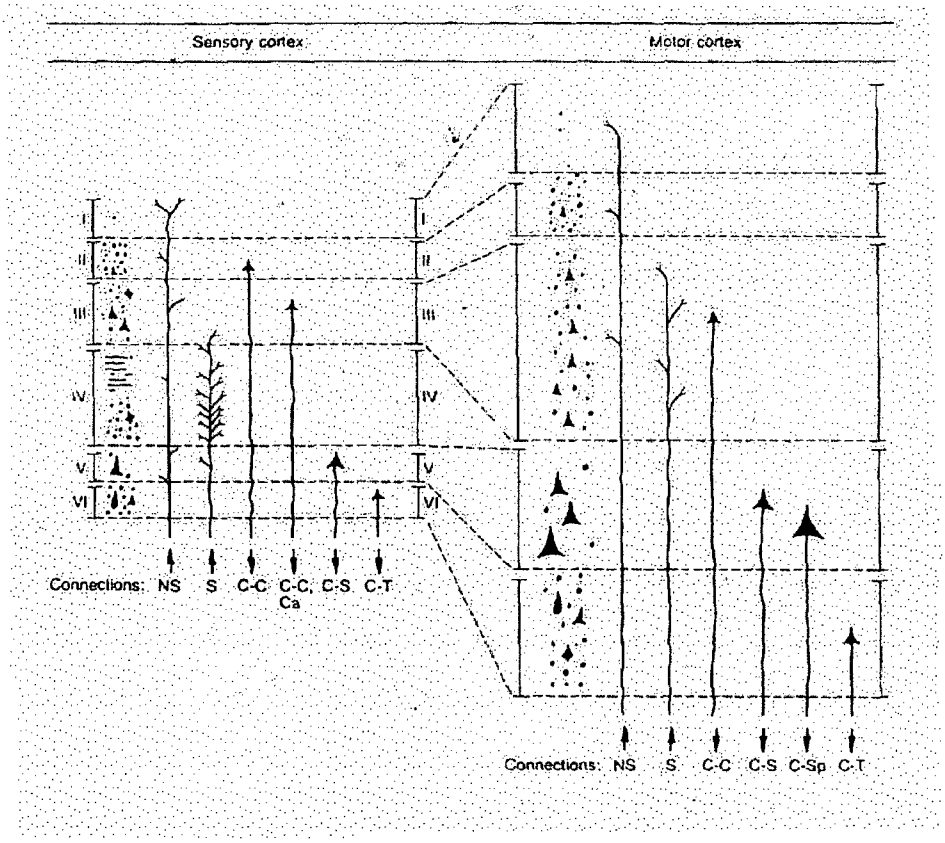

Figure 4-2. Efferent and afferent projections to the different cortical layers within the sensory and motor cortex.

Each layer within the neocortex has different efferent and afferent projections. Non-specific (NS) connections to the sensory cortex modulated by monoamine neurotransmitters terminate in all 6 layers of the cortex, whereas specific sensory (S) afferents (visual, auditory, somatosensory) synapse primarily on spiny stellate neurons in layer 4 in the sensory cortex. Those cells which have their somas in layers 2/3 are cortico-cortical efferents that project by means of the corpus callosum (C-C, Ca), whereas cells in layer 5 project mainly to the striatum (C-S) and those in layer 6 project to the thalamus (C-T). Connections within the motor cortex are similar to those within the sensory cortex with slight disparities. There are no projection neurons within layer 2 of the motor cortex and there is a population of cells in layer 5 of the motor cortex that project to the spinal cord (C-Sp). (figure adapted from O'Leary and Koester, 1993)

4.4. Selective damage to layer 5 neuron axons

Oxidative stress causes the disruption of cytoskeletal components such as microtubules, resulting in the termination of axonal transport, thus causing swelling and beading of axons. As

such, axonal beading has been shown to be a response to anoxic conditions *in vitro* (Tekkok et al., 2005) and to oxidative damage in human cultured brain tissue (Roediger and Armati, 2003). Here, we report moderately beaded axons at 2 h after stroke and a subsequent increase in the level of axonal beading with time after the ischemic insult. It was expected that the level of axonal damage would increase with time after ischemia as excitotoxicity is known to trigger a cascade of cellular events that continue to damage cells well beyond the time of initial insult (Dirnagl et al., 1999). We do not expect that damage to axons would increase beyond the 10 h time point, as there seemed to be a near complete loss of axonal integrity at this time. Our analysis of the incidence of beaded axons extending from layer 5 neurons located adjacent to the stroke core indicated that the spatial spread of ischemic damage to axons extended further laterally than the damage seen within the apical dendrites of these same neurons (Fig. 4-3). There are numerous possibilities as to why this was so, however at this time they remain speculative and require further investigation.

A first possibility is that the inherent physiology of axons make then more susceptible to ischemia than dendrites. As mentioned before, processes with a higher surface area to volume ratio such axons may not be able to buffer aberrant ion fluxes as efficiently as somatic compartments and larger dendrites thus making them more susceptible to excitotoxicity. This could explain why the axons of layer 5 neurons at the ischemic border appeared to be more damaged than nearby proximal dendrites. Further, a series of reports have shown that oligodendrocytes contain glutamate receptors (Agrawal and Fehlings, 1997; Rosenberg et al., 1999) and these are associated with the sensitivity of white matter tracts to excitotoxic and anoxic damage when studied *in vitro* (Li and Stys, 2000; Karadottir et al., 2005; Micu et al., 2006).

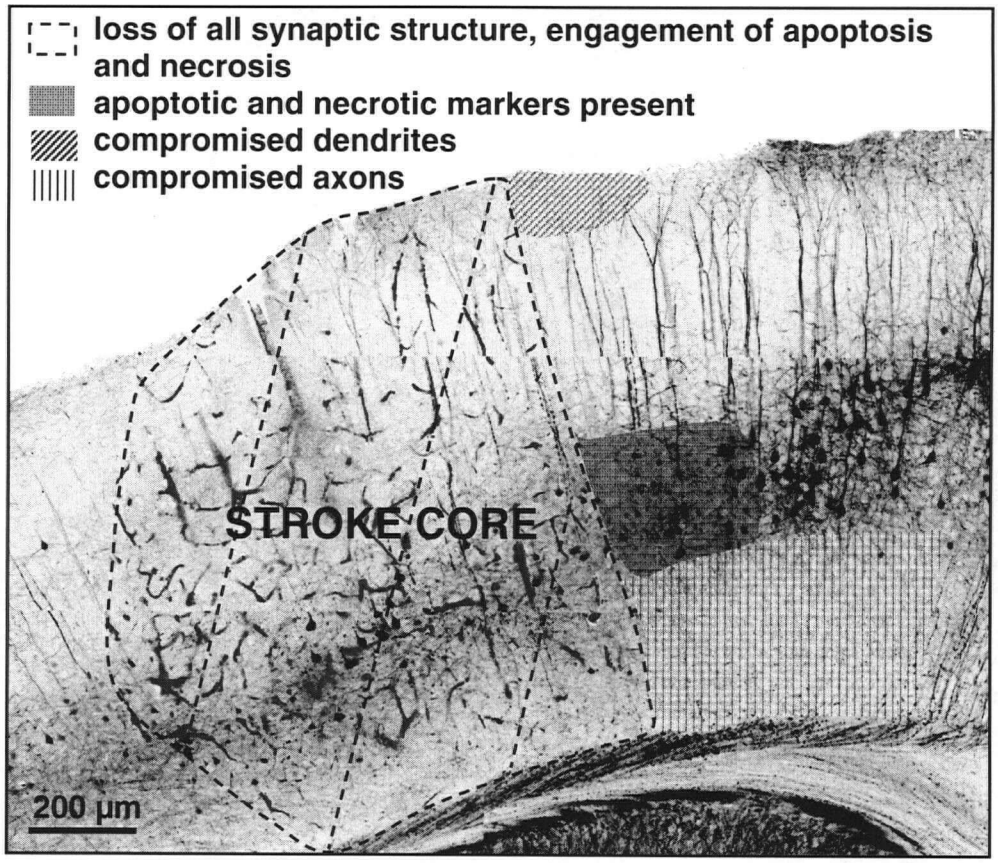

Figure 4-3. Spatial map of regions of complete and partial ischemic damage in relation to the location of ischemia.

Grayscale inverted image of a coronal section of a YFP mouse 6 h after stroke showing trapped TR-dextran in ischemic vessels *(red)*. The stroke core, *(dashed lines)* is a region of irreversibly damaged synaptic structure and engagement of apoptotic and necrotic cell death cascades. Apoptotic and necrotic markers are also found predominantly within the first 300 µm outside the stroke core *(grey shading)*. Ischemic damage was most apparent within the apical tuft dendrites of layer 5 neurons, and was most concentrated within 200 µm of the ischemic border *(horizontal hatching)*. Ischemic damage to the axons of layer 5 neurons extended further laterally than damage to dendrites, up to 600 µm beyond the stroke core *(vertical hatching)*.

Another possibility is that the cellular cascades initiated by excitotoxic damage could lead to the activation of a second messenger within the cortical tuft dendrites which acts as a retrograde signal, surpassing the proximal region of the dendrite as well as the cell soma, selectively affecting the axon. The nature of this retrograde signal could be a molecule intrinsic to the neuronal compartment such as a cytosolic protease; however, more likely is that this is a diffusible cytotoxic factor released from those neurons that have entered a stage of cell death. Since dendritic arbors project up to 200 μm laterally throughout the most superficial regions of the cortex this could account for the unexpected observation of axons being damaged in regions well outside the ischemic zone.

Finally, the increased incidence of beaded axons up to 600 μm away from the ischemic core could reflect intracortical back projections from damaged neurons within the stroke core up to interneurons located in other laminae in the penumbral tissue (Bannister, 2005). We believe that this is not the case, however, as we have investigated this possibility by tracking individual axons from neurons located within the stroke core as well as in the adjacent penumbra. It would appear that most of these axons branch upon entering the corpus callosum where they continue to project to their distal subcortical targets.

4.5. Evidence for activation of cell death mechanisms within peri-infarct zones

Immunohistological analysis of YFP neurons located in peri-infarct tissue revealed that neurons with condensed nuclei as well as activated caspase-3 and calpain-cleaved-α-spectrin staining were concentrated within 300 μm outside the ischemic core (Fig. 4-3). Beyond this distance, the nucleus size of YFP neurons did not differ from YFP neurons located on the non-ischemic hemisphere and there was a significant reduction (~50%) in the number of cells that exhibited markers of apoptosis or necrosis.

The spatial distribution of apoptotic and necrotic indices has been a matter of debate in ischemia. Some studies report a predominance of apoptotic markers in penumbral tissue (Namura et al., 1998; Sasaki et al., 2000; Benchoua et al., 2001) with necrotic markers being localized to the infarct core (Ferrer and Planas, 2003; Xu et al., 2006). It is understandable that the apoptotic cell death cascade might be inactivated within the stroke core as apoptosis is an ATP dependent mechanism and there is a rapid depletion of sources of ATP after ischemia within the infarct core (Yamashima, 2004). More recent findings, however, suggest that the location of these types of cell death are not so easily dissociated and depend on the nature and timing of the ischemic insult (Benchoua et al., 2001).

Here we report evidence for both markers of apoptosis and necrosis 6 h after ischemia and we show that these are found in both the stroke core and penumbra. The fact that up to 90% of neurons within 300 μm from the ischemic zone stained for both markers of apoptosis and necrosis suggests that these two forms of cell death might have been occurring simultaneously within the same population of layer 5 neurons. This is supported by evidence from another study where apoptotic and necrotic markers were shown to be expressed within the same set of ischemic neurons after transient and permanent MCA occlusion (Unal-Cevik et al., 2004). Further evidence for apoptosis in the ischemic penumbra has come from another model of focal ischemia (MCAO) where active caspase-3 labeling was found to be present specifically in the striatum but not cortex at 3 h and 6 h post reperfusion (Davoli et al., 2002). Yet another study noted a ring of apoptotic cell death is tissue immediately adjacent to the lesion site after a modified version of the MCAO stroke model which created a lesion specifically within functionally defined areas of the rat somatosensory cortex (Katsman et al., 2003). Thus, it

appears that post-ischemic neuronal death may involve a combination of apoptotic and necrotic processes even at the level of the individual neuron.

In our study, the localized activation of apoptotic and necrotic mechanisms within the first 300 μm of cortex adjacent to the lesion site suggests that this is an ideal site where delayed administration of potential anti-apoptotic agents (Wang et al., 2002) could rescue cells from progression to death. We cannot say with certainty whether or not cells that have initiated the apoptotic or necrotic death cascade are in fact in a salvageable state; however, evidence from another study showed that cells with activated caspase-3 were also immunreactive for NeuN (Davoli et al., 2002) suggesting that they were still viable and thus in a position to be rescued from cell death.

4.6. Dendritic beading as a sign of neuronal compromise

Focal bead-like swelling in dendrites and axons is thought to be a neuropathological sign of ischemia (Hori and Carpenter, 1994). Evidence shows that dendritic beading can be a reversible phenomenon (Kirov et al., 2004; Zhang et al., 2005) associated with neuronal cell dysfunction and in some cases can precede cell death (Ikegaya et al., 2001; Takeuchi et al., 2005). Despite this evidence, the functional state of dendrites with beaded morphology is still not known; however, preliminary data from our lab indicates that regions with beaded dendrites are not inactive as assessed by analysis of sensory-evoked intrinsic optical signals (in preparation Zhang et al.).

Here we report that up to 90% of neurons within the first 300 μm outside of the ischemic core showed apoptotic and necrotic markers within 6 h after stroke onset. Since most of these neurons had beaded dendrites (in particular within the first 100 μm) we would expect that

dendritic beading might be an early sign of cell death pathway involvement. As more cells with beaded apical tuft dendrites were found closer to the ischemic core, this might suggest that these cells were further along in their commitment to cell death. Thus neurons with beaded dendrites may represent a population of cells that have become functionally impaired due to glutamate excitotoxicity or energy failure but remain potentially viable, albeit with altered synaptic circuitry. Since anti-apoptotic treatments can rescue neurons even after ischemia it is unclear whether immunoreactive markers for signs of apoptosis or necrosis necessarily reflect an absolute commitment to cell death.

It should also be mentioned that layer 5 YFP neurons that seemed to be undergoing apoptosis or necrosis appeared to have retained little of their YFP fluorescence at the level of the cell body. Thus it is also plausible that early after the ischemic insult, dendritic beading may be an immediate response to ischemia, however with time and prolonged exposure to excitotoxic mechanisms, programs of cell death may become activated resulting in the breakdown of cytoskeletal components and deterioration of the YFP signal. This is supported by studies showing that ischemia triggers the activation of a number of proteolytic enzymes which lead to the breakdown of cytoskeletal and extracellular matrix proteins resulting in the loss of structural integrity (Dirnagl et al., 1999). Thus those cells that stained positively for markers of apoptotic and necrotic cell death may not have in fact coincided with those cells with beaded dendrites, as they no longer had the ability to retain their fluorescence. This brings about the possibility that our analysis of beaded dendrites underrepresented the population of cells that were damaged by excitoxicity; however, because we expressed beaded dendrites as a percentage of the total number of YFP dendrites within a 100 μm bin we believe we are properly representing the data. Further, we also counted the total number of dendrites on the non-ischemic hemisphere as a

control and found that this number did not differ significantly from the total number of dendrites (beaded + non-beaded) on the stroke side.

4.7. Conclusions

Using texas red-dextran caught within fixed ischemic vessels as a means of identifying ischemic zones we have finely mapped the spatial relationship between local blood flow and damage to the axonal and dendritic circuitry of layer 5 pyramidal neurons. Our data show that a sharp border exists between normal and damaged dendritic circuits within the ischemic penumbra 2 h, 6 h, and 10 h after stroke, despite the potential for diffusion of released cytotoxic factors from the dying core such as hemoglobin, glutamate, and nitric oxide. We also demonstrated that partially damaged neurons located along this border show a laminar distribution of damage throughout their length with compromised cortical tuft dendrites and axons but relatively intact proximal apical dendrites. Finally, apoptotic and necrotic cell death cascades appeared to be activated 6 h after stroke, however, only within 300 μm of the edge of the ischemic core. These data suggest that peri-infarct tissues 300 μm outside of an ischemic zone can be relatively free of dendritic damage and nuclear abnormalities suggesting that they may be in an ideal position to contribute to recovery of function after stroke.

4.8. Directions for future research

The findings in this study were mainly based on histological evidence of the morphological changes that occur to layer 5 neuron dendrites and axons after cerebral ischemia. It was surprising to find that not all regions of the layer 5 neuron dendrites responded similarly to ischemic damage. We can only speculate as to why the cortical tuft dendrites would be more susceptible to ischemic damage than the apical dendrites; hence it would be of interest to further investigate the mechanisms that exist to generate a laminar distribution of ischemic damage to

dendrites. The fact that ischemic damage to the axons of layer 5 neurons extended further laterally than damage to the dendrites of the same neurons was also surprising. Based on the analysis of confocal images with an axonal damage rating scale, it was quite clear that this was the case; however, the dense distribution of axons made it difficult to evaluate beading within individual axonal processes. Thus, it would be useful to provide further evidence for axonal damage with another methodological tool. There are antibodies that exist, such as SMI-32 (Sternberger Monoclonals), that stain for the non-phosphorylated form of monofilament H and such an antibody could be used to detect damaged axons within the brain after ischemia. Such evidence could strengthen our argument for enhanced sensitivity of axons to ischemic damage. Finally, as discussed earlier, it is not clear whether cells within the penumbra region that stained for markers of apoptosis and necrosis at 6 h after stroke would progress to the point of no return (ie. death) with time. Hence, a neuronal marker such a NeuN would be useful to determine whether or not these cells were still viable and thus could potentially be rescued from death with an anti-apoptotic treatment.

REFERENCES

American Heart Association, Heart Disease and Stroke Statistics Update 2006. http://www.americanheart.org/presenter.jhtml?identifier=3000090

Aarts M, Iihara K, Wei WL, Xiong ZG, Arundine M, Cerwinski W, MacDonald JF, Tymianski M (2003) A key role for TRPM7 channels in anoxic neuronal death. Cell 115:863-877.

Aarts MM, Tymianski M (2005) TRPM7 and Ischemic CNS Injury. Neuroscientist 11:116-123.

Aggoun-Zouaoui D, Margalli I, Borrega F, Represa A, Plotkine M, Ben-Ari Y, Charriaut-Marlangue C (1998) Ultrastructural morphology of neuronal death following reversible focal ischemia in the rat. Apoptosis 3:133-141.

Agrawal SK, Fehlings MG (1997) Role of NMDA and Non-NMDA Ionotropic Glutamate Receptors in Traumatic Spinal Cord Axonal Injury. J Neurosci 17:1055-1063.

Albensi BC, Knoblach SM, Chew BG, O'Reilly MP, Faden AI, Pekar JJ (2000) Diffusion and high resolution MRI of traumatic brain injury in rats: time course and correlation with histology. Exp Neurol 162:61-72.

Andrew RD, Jarvis CR, Obeidat AS (1999) Potential Sources of Intrinsic Optical Signals Imaged in Live Brain Slices. Methods 18:185-196.

Ashton D, Willems R, Marrannes R, Janssen PAJ (1990) Extracellular ions during veratridine-induced neurotoxicity in hippocampal slices: neuroprotective effects of flunarizine and tetrodotoxin. Brain Research 528:212-222.

Bannister AP (2005) Inter- and intra-laminar connections of pyramidal cells in the neocortex. Neurosci Res 53:95-103.

Bederson JB, Germano IM, Guarino L (1995) Cortical blood flow and cerebral perfusion pressure in a new noncraniotomy model of subarachnoid hemorrhage in the rat. Stroke 26:1086-1091; discussion 1091-1082.

Bederson JB, Pitts LH, Tsuji M, Nishimura MC, Davis RL, Bartkowski H (1986) Rat middle cerebral artery occlusion: evaluation of the model and development of a neurologic examination. Stroke 17:472-476.

Belayev L, Alonso OF, Busto R, Zhao W, Ginsberg MD (1996) Middle cerebral artery occlusion in the rat by intraluminal suture. Neurological and pathological evaluation of an improved model. Stroke 27:1616-1622; discussion 1623.

Benchoua A, Guegan C, Couriaud C, Hosseini H, Sampaio N, Morin D, Onteniente B (2001) Specific Caspase Pathways Are Activated in the Two Stages of Cerebral Infarction. J Neurosci 21:7127-7134.

Benowitz LI, Routtenberg A (1997) GAP-43: an intrinsic determinant of neuronal development and plasticity. Trends Neurosci 20:84-91.

Biernaskie J, Corbett D (2001) Enriched Rehabilitative Training Promotes Improved Forelimb Motor Function and Enhanced Dendritic Growth after Focal Ischemic Injury. J Neurosci 21:5272-5280.

Carmichael ST (2003) Plasticity of cortical projections after stroke. Neuroscientist 9:64-75.

Carmichael ST (2005) Rodent models of focal stroke: size, mechanism, and purpose. NeuroRx 2:396-409.

Carmichael ST, Wei L, Rovainen CM, Woolsey TA (2001) New patterns of intracortical projections after focal cortical stroke. Neurobiol Dis 8:910-922.

Cauller L, Connors B (1994) Synaptic physiology of horizontal afferents to layer I in slices of rat SI neocortex. J Neurosci 14:751-762.

Chen J, Nagayama T, Jin K, Stetler RA, Zhu RL, Graham SH, Simon RP (1998) Induction of caspase-3-like protease may mediate delayed neuronal death in the hippocampus after transient cerebral ischemia. J Neurosci 18:4914-4928.

Cheng YD, Al-Khoury L, Zivin JA (2004) Neuroprotection for ischemic stroke: two decades of success and failure. NeuroRx 1:36-45.

Churchill JD, Tharp JA, Wellman CL, Sengelaub DR, Garraghty PE (2004) Morphological correlates of injury-induced reorganization in primate somatosensory cortex. BMC Neurosci 5:43.

Dancause N, Barbay S, Frost SB, Plautz EJ, Chen D, Zoubina EV, Stowe AM, Nudo RJ (2005) Extensive cortical rewiring after brain injury. J Neurosci 25:10167-10179.

Davalos D, Grutzendler J, Yang G, Kim JV, Zuo Y, Jung S, Littman DR, Dustin ML, Gan W-B (2005) ATP mediates rapid microglial response to local brain injury in vivo. 8:752-758.

Davoli MA, Fourtounis J, Tam J, Xanthoudakis S, Nicholson D, Robertson GS, Ng GY, Xu D (2002) Immunohistochemical and biochemical assessment of caspase-3 activation and DNA fragmentation following transient focal ischemia in the rat. Neuroscience 115:125-136.

Dietrich WD, Watson BD, Busto R, Ginsberg MD, Bethea JR (1987) Photochemically induced cerebral infarction. I. Early microvascular alterations. Acta Neuropathol (Berl) 72:315-325.

Dietrich WD, Feng ZC, Leistra H, Watson BD, Rosenthal M (1994) Photothrombotic infarction triggers multiple episodes of cortical spreading depression in distant brain regions. J Cereb Blood Flow Metab 14:20-28.

Dirnagl U, Iadecola C, Moskowitz MA (1999) Pathobiology of ischaemic stroke: an integrated view. Trends Neurosci 22:391-397.

Dittmar M, Spruss T, Schuierer G, Horn M (2003) External carotid artery territory ischemia impairs outcome in the endovascular filament model of middle cerebral artery occlusion in rats. Stroke 34:2252-2257.

Feng G, Mellor RH, Bernstein M, Keller-Peck C, Nguyen QT, Wallace M, Nerbonne JM, Lichtman JW, Sanes JR (2000) Imaging neuronal subsets in transgenic mice expressing multiple spectral variants of GFP. Neuron 28:41-51.

Ferrer I, Planas AM (2003) Signaling of cell death and cell survival following focal cerebral ischemia: life and death struggle in the penumbra. J Neuropathol Exp Neurol 62:329-339.

Ferrer I, Friguls B, Dalfo E, Justicia C, Planas AM (2003) Caspase-dependent and caspase-independent signalling of apoptosis in the penumbra following middle cerebral artery occlusion in the adult rat. Neuropathol Appl Neurobiol 29:472-481.

Floyd RA (1999) Antioxidants, oxidative stress, and degenerative neurological disorders. Proceedings of the Society for Experimental Biology and Medicine 222:236-245.

Frizzell JP (2005) Acute stroke: pathophysiology, diagnosis, and treatment. AACN Clin Issues 16:421-440; quiz 597-428.

Fujimura M, Morita-Fujimura Y, Murakami K, Kawase M, Chan PH (1998) Cytosolic redistribution of cytochrome c after transient focal cerebral ischemia in rats. J Cereb Blood Flow Metab 18:1239-1247.

Furlan M, Marchal G, Viader F, Derlon JM, Baron JC (1996) Spontaneous neurological recovery after stroke and the fate of the ischemic penumbra. Ann Neurol 40:216-226.

Gajkowska B, Frontczak-Baniewicz M, Gadamski R, Barskov I (1997) Photochemically-induced vascular damage in brain cortex. Transmission and scanning electron microscopy study. Acta Neurobiol Exp (Wars) 57:203-208.

Gill R, Andine P, Hillered L, Persson L, Hagberg H (1992) The effect of MK-801 on cortical spreading depression in the penumbral zone following focal ischaemia in the rat. Journal Of Cerebral Blood Flow And Metabolism: Official Journal Of The International Society Of Cerebral Blood Flow And Metabolism 12:371-379.

Ginsberg MD, Pulsinelli WA (1994) The ischemic penumbra, injury thresholds, and the therapeutic window for acute stroke. Ann Neurol 36:553-554.

Gonzalez CLR, Kolb B (2003) A comparison of different models of stroke on behaviour and brain morphology. European Journal of Neuroscience 18:1950-1962.

Gu W, Jiang W, Wester P (1999) A photothrombotic ring stroke model in rats with sustained hypoperfusion followed by late spontaneous reperfusion in the region at risk. Exp Brain Res 125:163-170.

Hasbani MJ, Schlief ML, Fisher DA, Goldberg MP (2001) Dendritic Spines Lost during Glutamate Receptor Activation Reemerge at Original Sites of Synaptic Contact. J Neurosci 21:2393-2403.

Hata R, Maeda K, Hermann D, Mies G, Hossmann KA (2000) Dynamics of regional brain metabolism and gene expression after middle cerebral artery occlusion in mice. J Cereb Blood Flow Metab 20:306-315.

Hausser M, Spruston N, Stuart GJ (2000) Diversity and Dynamics of Dendritic Signaling. Science 290:739-744.

Heo JH, Han SW, Lee SK (2005) Free radicals as triggers of brain edema formation after stroke. Free Radical Biology and Medicine 39:51-70.

Hori N, Carpenter DO (1994) Functional and Morphological Changes Induced by Transient in Vivo Ischemia. Experimental Neurology 129:279-289.

Hossmann KA (1994) Viability thresholds and the penumbra of focal ischemia. Ann Neurol 36:557-565.

Hossmann KA (1996) Periinfarct depolarizations. Cerebrovasc Brain Metab Rev 8:195-208.

Hossmann K-A (1998) Experimental models for the investigation of brain ischemia. Cardiovascular Research 39:106-120.

Hu X, Brannstrom T, Gu W, Wester P (1999) A photothrombotic ring stroke model in rats with or without late spontaneous reperfusion in the region at risk. Brain Res 849:175-186.

Hu X, Wester P, Brannstrom T, Watson BD, Gu W (2001) Progressive and reproducible focal cortical ischemia with or without late spontaneous reperfusion generated by a ring-shaped, laser-driven photothrombotic lesion in rats. Brain Res Brain Res Protoc 7:76-85.

Hurn PD, Vannucci SJ, Hagberg H (2005) Adult or Perinatal Brain Injury: Does Sex Matter? Stroke 36:193-195.

Iijima T, Mies G, Hossmann KA (1992) Repeated negative DC deflections in rat cortex following middle cerebral artery occlusion are abolished by MK-801: effect on volume of ischemic injury. Journal Of Cerebral Blood Flow And Metabolism: Official Journal Of The International Society Of Cerebral Blood Flow And Metabolism 12:727-733.

Ikegaya Y, Kim J-A, Baba M, Iwatsubo T, Nishiyama N, Matsuki N (2001) Rapid and reversible changes in dendrite morphology and synaptic efficacy following NMDA receptor activation: implication for a cellular defense against excitotoxicity. J Cell Sci 114:4083-4093.

Jarvis CR, Lilge L, Vipond GJ, Andrew RD (1999) Interpretation of intrinsic optical signals and calcein fluorescence during acute excitotoxic insult in the hippocampal slice. Neuroimage 10:357-372.

Johansson BB, Ohlsson A-L (1996) Environment, Social Interaction, and Physical Activity as Determinants of Functional Outcome after Cerebral Infarction in the Rat. Experimental Neurology 139:322-327.

Jones T, Schallert T (1994) Use-dependent growth of pyramidal neurons after neocortical damage. J Neurosci 14:2140-2152.

Jones TA, Schallert T (1992) Overgrowth and pruning of dendrites in adult rats recovering from neocortical damage. Brain Res 581:156-160.

Jones TH, Morawetz RB, Crowell RM, Marcoux FW, FitzGibbon SJ, DeGirolami U, Ojemann RG (1981) Thresholds of focal cerebral ischemia in awake monkeys. J Neurosurg 54:773-782.

Karadottir R, Cavelier P, Bergersen LH, Attwell D (2005) NMDA receptors are expressed in oligodendrocytes and activated in ischaemia. 438:1162-1166.

Kato H, Kogure K (1999) Biochemical and molecular characteristics of the brain with developing cerebral infarction. Cell Mol Neurobiol 19:93-108.

Katsman D, Zheng J, Spinelli K, Carmichael ST (2003) Tissue microenvironments within functional cortical subdivisions adjacent to focal stroke. J Cereb Blood Flow Metab 23:997-1009.

Katsura K, Kristian T, Siesjo BK (1994) Energy metabolism, ion homeostasis, and cell damage in the brain. Biochem Soc Trans 22:991-996.

Kirov SA, Petrak LJ, Fiala JC, Harris KM (2004) Dendritic spines disappear with chilling but proliferate excessively upon rewarming of mature hippocampus. Neuroscience 127:69-80.

Kleinfeld D, Denk W (2000) Imaging neurons: a laboratory manual. In. Cold Spring Harbor, NY: Cold Spring Harbor Laboratory.

Kleinfeld D, Mitra PP, Helmchen F, Denk W (1998) Fluctuations and stimulus-induced changes in blood flow observed in individual capillaries in layers 2 through 4 of rat neocortex. Proc Natl Acad Sci U S A 95:15741-15746.

Kristian T, Siesjo BK (1998) Calcium in ischemic cell death. Stroke 29:705-718.

Kuge Y, Minematsu K, Yamaguchi T, Miyake Y (1995) Nylon monofilament for intraluminal middle cerebral artery occlusion in rats. Stroke 26:1655-1657; discussion 1658.

Lee VM, Burdett NG, Carpenter A, Hall LD, Pambakian PS, Patel S, Wood NI, James MF (1996) Evolution of photochemically induced focal cerebral ischemia in the rat. Magnetic resonance imaging and histology. Stroke 27:2110-2118; discussion 2118-2119.

Li F, Omae T, Fisher M (1999) Spontaneous hyperthermia and its mechanism in the intraluminal suture middle cerebral artery occlusion model of rats. Stroke 30:2464-2470; discussion 2470-2461.

Li S, Stys PK (2000) Mechanisms of Ionotropic Glutamate Receptor-Mediated Excitotoxicity in Isolated Spinal Cord White Matter. J Neurosci 20:1190-1198.

Lipton P (1999) Ischemic Cell Death in Brain Neurons. Physiol Rev 79:1431-1568.

Lledo P-M, Alonso M, Grubb MS (2006) Adult neurogenesis and functional plasticity in neuronal circuits. 7:179-193.

Longa EZ, Weinstein PR, Carlson S, Cummins R (1989) Reversible middle cerebral artery occlusion without craniectomy in rats. Stroke 20:84-91.

Majno G, Joris I (1995) Apoptosis, oncosis, and necrosis. An overview of cell death. Am J Pathol 146:3-15.

Markgraf CG, Kraydieh S, Prado R, Watson BD, Dietrich WD, Ginsberg MD (1993) Comparative histopathologic consequences of photothrombotic occlusion of the distal middle cerebral artery in Sprague-Dawley and Wistar rats. Stroke 24:286-292; discussion 292-283.

Markgraf CG, Green EJ, Watson B, McCabe PM, Schneiderman N, Dietrich WD, Ginsberg MD (1994) Recovery of sensorimotor function after distal middle cerebral artery photothrombotic occlusion in rats. Stroke 25:153-159.

Martin RL, Lloyd HG, Cowan AI (1994) The early events of oxygen and glucose deprivation: setting the scene for neuronal death? Trends Neurosci 17:251-257.

Masaki T, Yanagisawa M (1992) Endothelins. Essays Biochem 27:79-89.

Mayo NE, Wood-Dauphinee S, Ahmed S, Gordon C, Higgins J, McEwen S, Salbach N (1999) Disablement following stroke. Disabil Rehabil 21:258-268.

Mayzel-Oreg O, Omae T, Kazemi M, Li F, Fisher M, Cohen Y, Sotak CH (2004) Microsphere-induced embolic stroke: an MRI study. Magn Reson Med 51:1232-1238.

Metz GA, Antonow-Schlorke I, Witte OW (2005) Motor improvements after focal cortical ischemia in adult rats are mediated by compensatory mechanisms. Behav Brain Res 162:71-82.

Micu I, Jiang Q, Coderre E, Ridsdale A, Zhang L, Woulfe J, Yin X, Trapp BD, McRory JE, Rehak R, Zamponi GW, Wang W, Stys PK (2006) NMDA receptors mediate calcium accumulation in myelin during chemical ischaemia. Nature 439:988-992.

Millan M, Davalos A (2006) The need for new therapies for acute ischaemic stroke. Cerebrovasc Dis 22 Suppl 1:3-9.

Miyake K, Takeo S, Kaijihara H (1993) Sustained decrease in brain regional blood flow after microsphere embolism in rats. Stroke 24:415-420.

Namura S, Zhu J, Fink K, Endres M, Srinivasan A, Tomaselli KJ, Yuan J, Moskowitz MA (1998) Activation and cleavage of caspase-3 in apoptosis induced by experimental cerebral ischemia. J Neurosci 18:3659-3668.

Nath R, Raser KJ, Stafford D, Hajimohammadreza I, Posner A, Allen H, Talanian RV, Yuen P, Gilbertsen RB, Wang et a (1996) Non-erythroid alpha-spectrin breakdown by calpain and interleukin 1 beta-converting-enzyme-like protease(s) in apoptotic cells: contributory roles of both protease families in neuronal apoptosis. The Biochemical Journal 319 (Pt 3):683-690.

Ng S-C, de la Monte SM, Conboy GL, Karns LR, Fishman MC (1988) Cloning of human GAP 43: Growth association and ischemic resurgence. Neuron 1:133-139.

Nimmerjahn A, Kirchhoff F, Helmchen F (2005) Resting Microglial Cells Are Highly Dynamic Surveillants of Brain Parenchyma in Vivo. Science 308:1314-1318.

Nudo RJ, Wise BM, SiFuentes F, Milliken GW (1996) Neural Substrates for the Effects of Rehabilitative Training on Motor Recovery After Ischemic Infarct. Science 272:1791-1794.

Ohlsson A-L, Johansson BB (1995) Environment Influences Functional Outcome of Cerebral Infarction in Rats. Stroke 26:644-649.

O'Leary DDM, Koester SE (1993) Development of projection neuron types, axon pathways, and patterned connections of the mammalian cortex. Neuron 10:991-1006.

Park CK, Nehls DG, Teasdale GM, McCulloch J (1989) Effect of the NMDA antagonist MK-801 on local cerebral blood flow in focal cerebral ischaemia in the rat. J Cereb Blood low Metab 9:617-622.

Park JS, Bateman MC, Goldberg MP (1996) Rapid Alterations in Dendrite Morphology during Sublethal Hypoxia or Glutamate Receptor Activation. Neurobiology of Disease 3:215-227.

Robinson RG, Shoemaker WJ, Schlumpf M, Valk T, Bloom FE (1975) Effect of experimental cerebral infarction in rat brain on catecholamines and behaviour. Nature 255:332-334.

Roediger B, Armati PJ (2003) Oxidative stress induces axonal beading in cultured human brain tissue. Neurobiology of Disease 13:222-229.

Rosamond WD, Folsom AR, Chambless LE, Wang C-H, McGovern PG, Howard G, Copper LS, Shahar E (1999) Stroke Incidence and Survival Among Middle-Aged Adults : 9-Year Follow-Up of the Atherosclerosis Risk in Communities (ARIC) Cohort. Stroke 30:736-743.

Rosenberg LJ, Teng YD, Wrathall JR (1999) 2,3-Dihydroxy-6-Nitro-7-Sulfamoyl-Benzo(f)Quinoxaline Reduces Glial Loss and Acute White Matter Pathology after Experimental Spinal Cord Contusion. J Neurosci 19:464-475.

Sasaki C, Kitagawa H, Zhang WR, Warita H, Sakai K, Abe K (2000) Temporal profile of cytochrome c and caspase-3 immunoreactivities and TUNEL staining after permanent middle cerebral artery occlusion in rats. Neurological Research 22:223-228.

Sayre LM, Perry G, Smith MA (1999) In situ methods for detection and localization of markers of oxidative stress: application in neurodegenerative disorders. Methods In Enzymology 309:133-152.

Schaffer CB, Friedman B, Nishimura N, Schroeder LF, Tsai PS, Ebner FF, Lyden PD, Kleinfeld D (2006) Two-Photon Imaging of Cortical Surface Microvessels Reveals a Robust Redistribution in Blood Flow after Vascular Occlusion. PLoS Biology 4.

Schmid-Elsaesser R, Zausinger S, Hungerhuber E, Baethmann A, Reulen HJ (1998) A critical reevaluation of the intraluminal thread model of focal cerebral ischemia: evidence of inadvertent premature reperfusion and subarachnoid hemorrhage in rats by laser-Doppler flowmetry. Stroke 29:2162-2170.

Schneider G, Fries P, Wagner-Jochem D, Thome D, Laurer H, Kramann B, Mautes A, Hagen T (2002) Pathophysiological changes after traumatic brain injury: comparison of two experimental animal models by means of MRI. Magma 14:233-241.

Shanina EV, Redecker C, Reinecke S, Schallert T, Witte OW (2005) Long-term effects of sequential cortical infarcts on scar size, brain volume and cognitive function. Behav Brain Res 158:69-77.

Sharp FR, Lu A, Tang Y, Millhorn DE (2000) Multiple Molecular Penumbras After Focal Cerebral Ischemia. 20:1011-1032.

Stroemer RP, Kent TA, Hulsebosch CE (1992) Increase in synaptophysin immunoreactivity following cortical infarction. Neurosci Lett 147:21-24.

Stroemer RP, Kent TA, Hulsebosch CE (1993) Acute increase in expression of growth associated protein GAP-43 following cortical ischemia in rat. Neurosci Lett 162:51-54.

Stroemer RP, Kent TA, Hulsebosch CE (1995) Neocortical neural sprouting, synaptogenesis, and behavioral recovery after neocortical infarction in rats. Stroke 26:2135-2144.

Takagi K, Zhao W, Busto R, Ginsberg MD (1995) Local hemodynamic changes during transient middle cerebral artery occlusion and recirculation in the rat: a [14C]iodoantipyrine autoradiographic study. Brain Res 691:160-168.

Takano J, Tomioka M, Tsubuki S, Higuchi M, Iwata N, Itohara S, Maki M, Saido TC (2005) Calpain mediates excitotoxic DNA fragmentation via mitochondrial pathways in adult brains: evidence from calpastatin mutant mice. J Biol Chem 280:16175-16184.

Takeuchi H, Mizuno T, Zhang G, Wang J, Kawanokuchi J, Kuno R, Suzumura A (2005) Neuritic Beading Induced by Activated Microglia Is an Early Feature of Neuronal Dysfunction Toward Neuronal Death by Inhibition of Mitochondrial Respiration and Axonal Transport. J Biol Chem 280:10444-10454.

Tamura A, Graham DI, McCulloch J, Teasdale GM (1981) Focal cerebral ischaemia in the rat: 1. Description of technique and early neuropathological consequences following middle cerebral artery occlusion. J Cereb Blood Flow Metab 1:53-60.

Tekkok SB, Faddis BT, Goldberg MP (2005) AMPA/kainate receptors mediate axonal morphological disruption in hypoxic white matter. Neuroscience Letters 382:275-279.

Traversa R, Cicinelli P, Pasqualetti P, Filippi M, Rossini PM (1998) Follow-up of interhemispheric differences of motor evoked potentials from the 'affected' and 'unaffected' hemispheres in human stroke. Brain Res 803:1-8.

Traystman RJ (2003) Animal models of focal and global cerebral ischemia. Ilar J 44:85-95.

Umemura K, Shimakura A, Nakashima M (1997) Neuroprotective effect of a novel AMPA receptor antagonist, YM90K, in rat focal cerebral ischaemia. Brain Res 773:61-65.

Unal-Cevik I, Kilinc M, Can A, Gursoy-Ozdemir Y, Dalkara T (2004) Apoptotic and necrotic death mechanisms are concomitantly activated in the same cell after cerebral ischemia. Stroke 35:2189-2194.

Urase K, Kouroku Y, Fujita E, Momoi T (2003) Region of caspase-3 activation and programmed cell death in the early development of the mouse forebrain. Brain Res Dev Brain Res 145:241-248.

Van Hoecke M, Prigent-Tessier A, Bertrand N, Prevotat L, Marie C, Beley A (2005) Apoptotic cell death progression after photothrombotic focal cerebral ischaemia: effects of the lipophilic iron chelator 2,2'-dipyridyl. Eur J Neurosci 22:1045-1056.

Wang F, Corbett D, Osuga H, Osuga S, Ikeda JE, Slack RS, Hogan MJ, Hakim AM, Park DS (2002) Inhibition of cyclin-dependent kinases improves CA1 neuronal survival and behavioral performance after global ischemia in the rat. J Cereb Blood Flow Metab 22:171-182.

Wang KK (2000) Calpain and caspase: can you tell the difference? Trends Neurosci 23:20-26.

Ward NS (2005) Mechanisms underlying recovery of motor function after stroke. Postgrad Med J 81:510-514.

Watson BD, Dietrich WD, Busto R, Wachtel MS, Ginsberg MD (1985) Induction of reproducible brain infarction by photochemically initiated thrombosis. Ann Neurol 17:497-504.

Weinstein PR, Hong S, Sharp FR (2004) Molecular identification of the ischemic penumbra. Stroke 35:2666-2670.

Wellman CL, Sengelaub DR (1995) Alterations in dendritic morphology of frontal cortical neurons after basal forebrain lesions in adult and aged rats. Brain Research 669:48-58.

Wester P, Watson BD, Prado R, Dietrich WD (1995) A photothrombotic 'ring' model of rat stroke-in-evolution displaying putative penumbral inversion. Stroke 26:444-450.

Witte OW, Bidmon H-J, Schiene K, Redecker C, Hagemann G (2000) Functional Differentiation of Multiple Perilesional Zones After Focal Cerebral Ischemia. 20:1149-1165.

Wong-Riley MTT (1989) Cytochrome oxidase: an endogenous metabolic marker for neuronal activity. Trends in Neurosciences 12:94-101.

Wu W, Guan X, Zhang X, Kuang P (2002) GAP-43 expression and pathological changes of temporal infarction in rats and effects of batroxobin. J Tradit Chin Med 22:42-46.

Xerri C, Merzenich MM, Peterson BE, Jenkins W (1998) Plasticity of primary somatosensory cortex paralleling sensorimotor skill recovery from stroke in adult monkeys. J Neurophysiol 79:2119-2148.

Xu X-H, Zhang S-M, Yan W-M, Li X-R, Zhang H-Y, Zheng X-X (2006) Development of cerebral infarction, apoptotic cell death and expression of X-chromosome-linked inhibitor of apoptosis protein following focal cerebral ischemia in rats. Life Sciences 78:704-712.

Yamashima T (2004) Ca2+-dependent proteases in ischemic neuronal death: a conserved 'calpain-cathepsin cascade' from nematodes to primates. Cell Calcium 36:285-293.

Yamashima T, Tonchev AB, Tsukada T, Saido TC, Imajoh-Ohmi S, Momoi T, Kominami E (2003) Sustained calpain activation associated with lysosomal rupture executes necrosis of the postischemic CA1 neurons in primates. Hippocampus 13:791-800.

Yao H, Markgraf CG, Dietrich WD, Prado R, Watson BD, Ginsberg MD (1994) Glutamate antagonist MK-801 attenuates incomplete but not complete infarction in thrombotic distal middle cerebral artery occlusion in Wistar rats. Brain Res 642:117-122.

Zhang S, Boyd J, Delaney K, Murphy TH (2005) Rapid Reversible Changes in Dendritic Spine Structure In Vivo Gated by the Degree of Ischemia. J Neurosci 25:5333-5338.